

## Highlights

### **Integrating organic Rankine cycles for waste heat recovery from onboard diesel generators in the maritime sector: Simulation and techno-economic assessment**

Daniel Sánchez-Lozano, Roque Aguado, Antonio Escámez, José Antonio Hernández-Torres, Juan P. Torreglosa, David Vera

- Acetone and cyclopentane are identified as the best-performing working fluids.
- Off-design evaluation with acetone at 85% load yields a net electrical efficiency of 8.45%.
- Real-route analysis indicates an 18.5% annual reduction in carbon dioxide emissions.
- The system breaks even in 11.7 years, reaching an internal rate of return of 12.8%.
- A sensitivity analysis of the organic Rankine cycle unit's economic viability is included.

# Integrating organic Rankine cycles for waste heat recovery from onboard diesel generators in the maritime sector: Simulation and techno-economic assessment

Daniel Sánchez-Lozano<sup>a</sup>, Roque Aguado<sup>a,\*</sup>, Antonio Escámez<sup>a</sup>, José Antonio Hernández-Torres<sup>b</sup>, Juan P. Torreglosa<sup>b</sup>, David Vera<sup>a</sup>

<sup>a</sup>*Departamento de Ingeniería Eléctrica, Escuela Politécnica Superior de Linares, Universidad de Jaén, Avda. de la Universidad s/n, 23700 Linares, Spain*

<sup>b</sup>*Departamento de Ingeniería Eléctrica y Térmica, de Diseño y Proyectos, Escuela Técnica Superior de Ingeniería, Universidad de Huelva, Avda. de las Fuerzas Armadas s/n, 21007 Huelva, Spain*

---

## Abstract

The maritime sector's dependence on fossil fuels, coupled with the rising crude oil prices, underscores the urgent need to enhance ship efficiency and advance the decarbonization of the marine sector. This paper evaluates the technical and economic feasibility of integrating organic Rankine cycle (ORC) systems in diesel-electric propulsion marine distribution vessels. A comprehensive simulation and optimization of a 1.6 MW ORC unit, using acetone as the working fluid, has been conducted. The system is designed to recover waste heat from the exhaust gases of diesel generators aboard a vessel. Under an 85% load of the diesel generators, the ORC bottoming unit demonstrates a net electrical efficiency of 8.45% with a thermodynamic cycle efficiency of 18.73%. It is estimated that this system could reduce annual carbon dioxide emissions and diesel fuel consumption by 18.5% compared to conventional systems. From a financial perspective, assuming a conservative discount rate of 8%, the ORC system demonstrates long-term viability with a cumulative profit of 44% on the initial investment, a payback period of 11.7 years, and an internal rate of return of 12.8%. Additionally, the advantages of integrating the ORC technology with direct current distribution networks are highlighted, simplifying system architecture and improving energy efficiency.

**Keywords:** Organic Rankine cycle, Waste heat recovery, Maritime sector, Hybrid electric propulsion, Working fluid selection, Sensitivity analysis

---

---

\*Corresponding author

*Email addresses:* dslozano@ujaen.es (Daniel Sánchez-Lozano), ramolina@ujaen.es (Roque Aguado), aescamez@ujaen.es (Antonio Escámez), joseantonio.hernandez@dimme.uhu.es (José Antonio Hernández-Torres), juan.perez@die.uhu.es (Juan P. Torreglosa), dvera@ujaen.es (David Vera)

## 1. Introduction

The rising crude oil prices are motivating shipping industries to improve vessel efficiency and reduce their dependency on fossil fuels [1]. As the global gross domestic product grows, the maritime sector is experiencing an increase in energy demand [2]. According to estimates by the International Maritime Organization (IMO) [3], the shipping sector emitted a total of 1,056 million tonnes of CO<sub>2</sub> in 2018, accounting for approximately 2.89% of anthropogenic CO<sub>2</sub> emissions. International shipping contributes to only about 9% of the global emissions related to the transport sector [3]. However, a 40–115% growth is expected in the maritime trade sector by 2050 in comparison to 2020 levels [3]. Nowadays, approximately 99% of international shipping's energy demand is met by fossil fuels, with fuel oil and marine gas oil (MGO) accounting for up to 95% of the total demand [2]. Therefore, urgent action is imperative to accelerate the energy transformation, promote sustainability, and achieve decarbonization of the sector. Otherwise, the IMO warns that greenhouse gas (GHG) emissions associated with shipping could increase by 50–250% by 2050 compared to 2008 emission levels [2]. The shipping industry is currently focusing on decarbonization through electrification. Inspired by trends in the automotive industry, hybrid electric propulsion systems are increasingly being proposed and used on ships to achieve greater energy efficiency [4].

Currently, the majority of electric propulsion systems used in vessels are based on an alternating current (AC) distribution network. Despite their widespread use, they present significant drawbacks in their application, such as the need to synchronize generation units, manage reactive power flow, control transformer starting currents, handle harmonic currents, mitigate three-phase imbalances [5], and reduce system efficiency, as motors operate at a constant speed [6]. Due to these challenges and the recent advancements in the field of semiconductors [7], a transformation is underway in the maritime sector through the implementation of direct current (DC) distribution systems. In DC distribution, the mechanical energy generated by diesel engines is converted into electricity in AC through synchronous generators. AC is converted to DC through rectifiers

27 connected to the DC distribution network. For propulsion, the propellers are connected to the DC  
28 network through sets of inverter controllers and induction machines [8]. For the connection of AC  
29 loads, inverters are used, which may be connected to transformers to adjust the output voltage, if  
30 necessary.

31 A DC distribution system offers several advantages. Firstly, it reduces the number of conver-  
32 sion stages, simplifying the system architecture [8]. Secondly, it enables weight reduction and  
33 a more flexible equipment arrangement [5]. Additionally, synchronization units are unnecessary,  
34 streamlining design and operation [9]. Furthermore, it enhances energy efficiency by optimizing  
35 generation system operation, leading to reduced fuel consumption and emissions. Moreover, the  
36 system minimizes noise and decreases mechanical and thermal loads on the engine [10]. It also  
37 facilitates the integration of renewable energies and the implementation of storage systems [5].  
38 Lastly, its robustness against failures is ensured by power electronics, allowing immediate control  
39 of the electrical variables to prevent failures from spreading through the network and disturbing  
40 voltage and frequency [10].

41 The main sources of thermal energy that can be harnessed in ships include the exhaust gases  
42 generated by the engines and cooling flows [11]. Indeed, a substantial fraction, around 50%, of  
43 the total thermal energy contained in the fuel is dissipated as heat [12]. It is noteworthy that about  
44 26% of this thermal energy is contained in the exhaust gases [12].

45 Organic Rankine cycles (ORC) are innovative systems that utilize organic fluids to achieve  
46 higher efficiencies in recovering heat at temperatures below 400 °C [13]. Most studies on ORC  
47 systems have largely focused on industrial applications [14], with limited exploration of their use  
48 in maritime settings. Ongoing research is now focused on the application of ORC units for re-  
49 covering waste heat in ships, where its potential to reduce fuel consumption and CO<sub>2</sub> emissions  
50 in maritime transport is significant, driven by the need to adapt ships to new regulations. Re-  
51 cent publications have assessed the feasibility of ORC units for recovering residual heat in marine  
52 diesel engines. These systems are promising alternatives for efficiently recovering heat at lower

53 temperatures, and active efforts are currently underway to optimize this technology for implemen-  
54 tation in the maritime sector [12, 14–18]. For example, Konur et al. [19] analyzed an ORC system  
55 for recovering waste heat from exhaust gases in the marine diesel generators of an oil/chemical  
56 tanker. The system was thermodynamically modeled, resulting in the optimization of the organic  
57 fluid, with R1336mzz(Z) being selected. This optimization led to a 15% reduction in fuel usage,  
58 resulting in an annual reduction of emissions totaling 849.63 t CO<sub>2</sub>, 6.96 t SO<sub>x</sub>, and 24.79 t NO<sub>x</sub>.  
59 In addition, Yang et al. [20] evaluated a waste heat recovery (WHR) system applying an ORC  
60 system with R245fa as organic working fluid, achieving annual savings of 489,000 kg of diesel  
61 fuel, resulting in a 76% reduction in CO<sub>2</sub> emissions per kWh generated compared to the conven-  
62 tional diesel scenario. Pallis et al. [21] utilized jacket cooling water to design and manufacture  
63 a small-scale prototype of a marine ORC heat recovery system. R134a was chosen as the work-  
64 ing fluid, with 2500 kW<sub>th</sub> available from the cooling water, resulting in a net electric power of  
65 170 kW<sub>e</sub>. With this electrical power output, a total electricity generation of 1145 MWh<sub>e</sub> can be  
66 produced annually if the system operates continuously. Zeng et al. [22] devised an ORC system  
67 to harness all the available heat sources from a ship, including exhaust gases, scavenged air, and  
68 jacket cooling water waste heat. R245fa was used as the working fluid. Their findings revealed  
69 that this technology allowed for an increase in the net output power of the system from 431 W to  
70 526 W. Finally, ChunWee et al. [23] addressed the implementation of ORC units in marine vessels  
71 for WHR, focusing on an offshore service vessel. The economic analysis indicated a potential  
72 annual fuel savings of 5 to 9%, with a specific installation cost of \$5000-8000 \$/kW. The ORC  
73 in a simple cycle configuration with methanol as the working fluid exhibited the shortest payback  
74 period. Additionally, an entropy generation analysis was conducted, emphasizing the importance  
75 of improving heat exchangers to reduce entropy generation.

76 The main novelty of the proposed approach lies in the detailed simulation, off-design optimiza-  
77 tion, and techno-economic assessment of an ORC unit tailored for marine diesel-electric propul-  
78 sion, utilizing advanced DC distribution networks. By harnessing the thermal energy available in

79 the exhaust gas from diesel generators, this study demonstrates significant potential for reducing  
80 fuel consumption and emissions, thereby contributing to the decarbonization goals of the maritime  
81 sector. This work incorporates off-design optimization, an essential yet underutilized technique,  
82 to assess the ORC system's performance under varying load conditions on actual ship routes.  
83 Additionally, very few studies in the scientific literature have conducted comprehensive techno-  
84 economic assessments of onboard ORC systems. This research provides a comparative analysis  
85 that considers both technical performance and economic viability, including a detailed sensitivity  
86 analysis, which is essential for practical implementation. Moreover, economic and emissions anal-  
87 ysis is based on real ship routes, a perspective that has been largely overlooked in the literature.  
88 Lastly, the integration of ORC units in modern DC distribution networks on ships remains highly  
89 underexplored in scientific research. This paper addresses this gap, demonstrating the benefits of  
90 using DC systems to improve energy efficiency and reduce greenhouse gas emissions.

91 The remainder of this article is structured as follows. Section 2 introduces the case study on the  
92 application of ORC systems in diesel-electric propulsion in ships, as well as a description of the  
93 software used to simulate the integrated ORC system, the underlying assumptions of the model,  
94 and the calculation methods. Section 3 provides an in-depth performance analysis of the ORC  
95 system, including a screening and comparison of various working fluids, their efficiencies, and  
96 thermodynamic behavior under different operating conditions, as well as a comprehensive evalua-  
97 tion using an elaborately designed Sankey diagram to illustrate energy flows and system efficiency.  
98 This section also investigates the off-design performance of the ORC system and its performance  
99 under typical conditions, in addition to an assessment of the energy efficiency of a cruise ship's ac-  
100 tual route, including the effect of integrating an ORC system on fuel consumption and emissions.  
101 An extensive economic feasibility assessment of the proposed ORC system, including a detailed  
102 sensitivity analysis, is also provided at the end of this section. Finally, a few concluding remarks  
103 are presented in Section 4.

## 104 **2. Methods**

105 In this section, the case study is first introduced, providing the context and operating condi-  
106 tions under which the ORC system is evaluated. Subsequently, the procedure for selecting the  
107 most suitable organic and heat transfer fluids is described, considering their thermodynamic prop-  
108 erties, environmental impact, and compatibility within the simulation framework. Afterwards, the  
109 mathematical model used for system analysis is presented, incorporating key aspects such as heat  
110 transfer efficiency and design parameters. Finally, the approach for the economic study is out-  
111 lined, detailing the financial formulas and the framework to assess the economic feasibility of the  
112 system.

113 In this case study, the integration of an ORC unit into the marine diesel propulsion system of a  
114 shuttle tanker is investigated. The main goal is to explore the potential benefits of utilizing waste  
115 heat recovery through ORC technology to enhance energy efficiency and reduce fuel consumption  
116 in marine applications. The selected case study vessel is a single-screw shuttle tanker, which is  
117 equipped with dual diesel generators that provide the necessary power for propulsion in a DC  
118 distribution system.

119 For simulation and optimization of the ORC system for marine diesel DC propulsion systems,  
120 the simplified model shown in Fig. 1 is used, based on the electrical layout of a single-screw shuttle  
121 tanker with propulsion [24], commonly used on real ships. The model consists of two zones.  
122 Each zone represents the installation of two energy systems composed of two diesel generators,  
123 specifically using the 12V46F model from the manufacturer Wärtsilä (Finland), which delivers a  
124 full load electrical power of 14.4 MW (18 MVA). In practice, one of the generation systems is  
125 installed on the port side and the other on the starboard side [25], with two diesel generators in  
126 each zone. This results in a net energy generation at full load of 57.6 MW (72 MVA). The scheme  
127 is complemented by the inclusion of rectifiers to convert the AC power from the diesel generator  
128 into DC power, as well as inverters to supply the propulsion system with AC.

129 The simulation of diesel generators is the starting point of this study. The technical features of

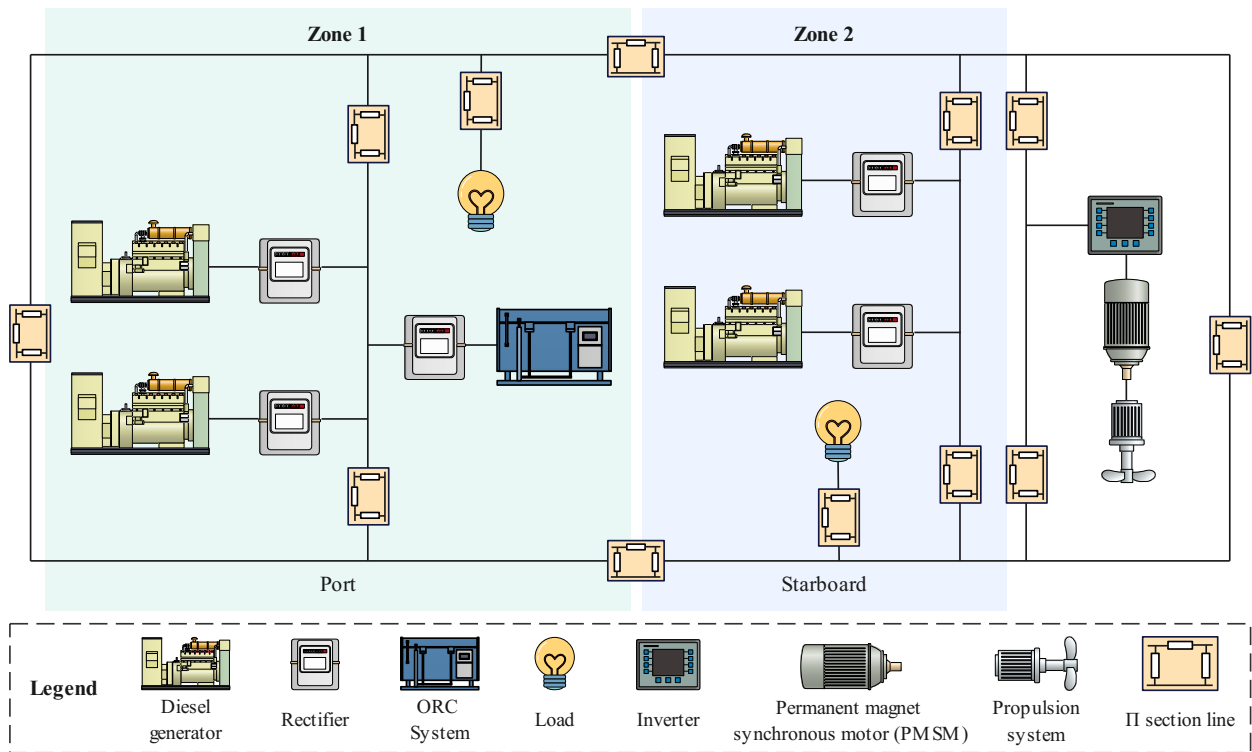


Figure 1: Schematic diagram of the DC propulsion vessel selected for the application of the ORC system.

130 the 12V46F marine diesel generator manufactured by Wärtsilä are reported in Table 1.

131 The integrated ORC system proposed in the study, shown in Fig. 2, consists of two ORC units  
 132 placed on the bow and the starboard. Consequently, the study only considers two of the four  
 133 available diesel generators. For hot sanitary water (HSW) production, the same engine cooling  
 134 water circuit is utilized. Regarding the ORC system, it comprises a mixer where the two exhaust  
 135 gas pipes from the diesel generators are combined. The combined exhaust gas flows through a  
 136 high-temperature heat exchanger (HTHX) where the gases transfer heat to a heat transfer fluid  
 137 loop, recommended to prevent potential local overheating and chemical instability of the organic  
 138 fluid. Subsequently, in an evaporator, the organic working fluid (WF) is heated before passing  
 139 through the expander to generate electrical energy. As the WF exits the expander, it passes through  
 140 a regenerator designed to extract some of the available heat from the WF and transfer it back to  
 141 the previous stage before entering the evaporator. Finally, the WF passes through a condenser that

Table 1: Representative characteristics of Wärtsilä 12V46F diesel generator for offshore applications [26].

Parameter		Value	Unit
Electrical power output (AC)		14.4	MW <sub>e</sub>
Angular speed		600	rpm
Combustion air flow at 100% load		25.1	kg/s
Temperature after air cooler		50	°C
Exhaust gas system	Flow at 100% load	25.95	kg/s
	Flow at 85% load	22.44	kg/s
	Flow at 75% load	21.84	kg/s
	Flow at 50% load	17.40	kg/s
	Exhaust temperature 100% load	364	°C
	Exhaust temperature 85% load	330	°C
	Exhaust temperature 75% load	330	°C
	Exhaust temperature 50% load	297	°C
Fuel system	SFOC at 100% load	182.5	g/kWh <sub>e</sub>
	SFOC at 85% load	176.8	g/kWh <sub>e</sub>
	SFOC at 75% load	185.9	g/kWh <sub>e</sub>
	SFOC at 50% load	195	g/kWh <sub>e</sub>
Cooling water system	Water temperature inlet	74	°C
	Water temperature outlet	91–95	°C

142 utilizes seawater, further reducing its temperature before being introduced to the pump to increase  
 143 its pressure for continuous repetition of the cycle.

### 144 2.1. Selection of the organic working fluid and the heat transfer fluid

145 Selecting a suitable organic fluid is a critical aspect in the design and modeling of an ORC  
 146 system [27–30]. The choice of one working fluid over another significantly impacts cycle per-  
 147 formance and efficiency [27, 29–31], as well as thermodynamic and plant design parameters and  
 148 applicable safety requirements [27].

149 The selection of the appropriate working fluid largely depends on two main characteristics:  
 150 the heat source temperature [27, 30] and the ORC configuration [30, 31]. For these reasons,  
 151 it is important for the fluid to have suitable critical constants, low molecular complexity, and  
 152 a boiling point compatible with the condenser [27]. Additionally, other important aspects such

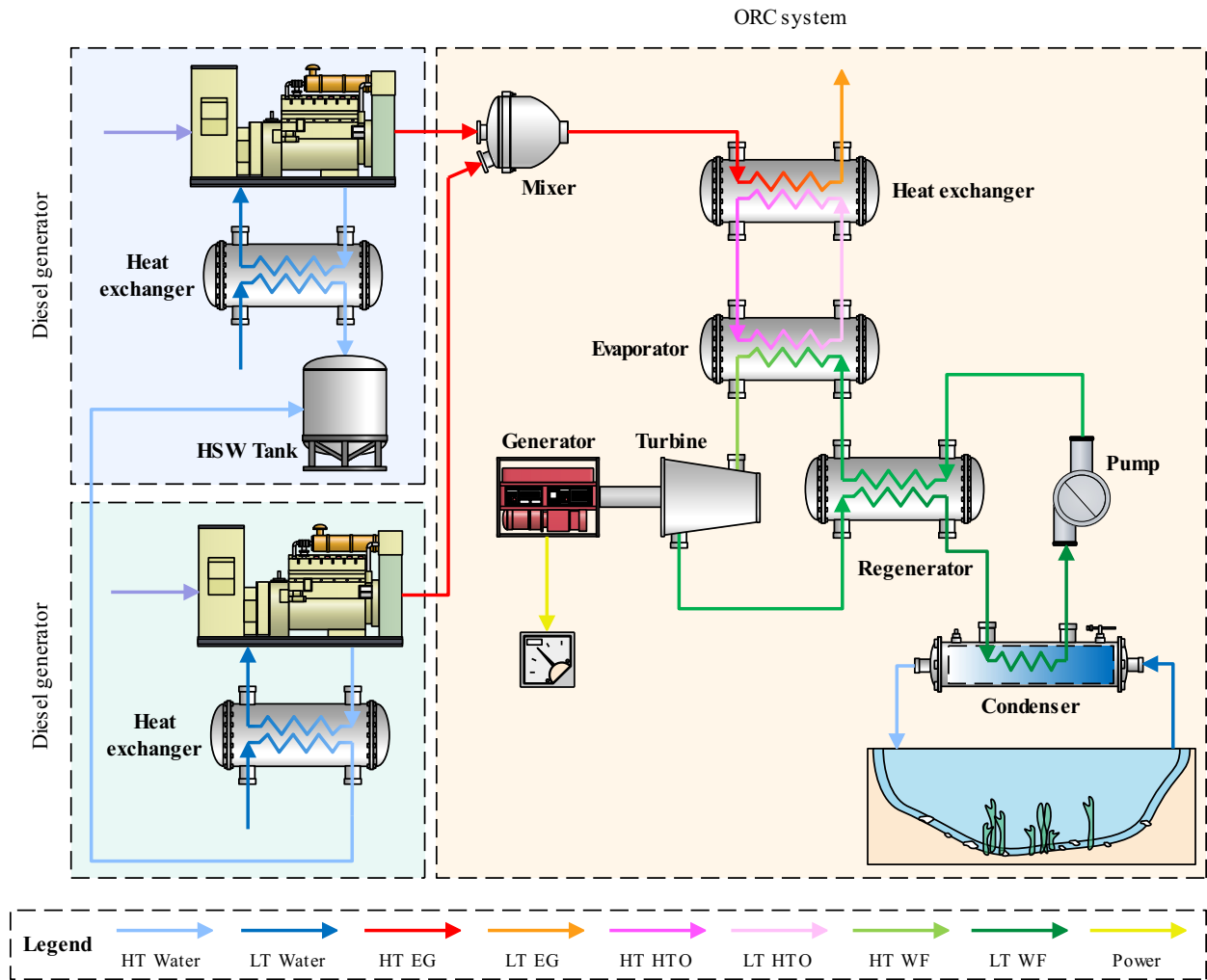


Figure 2: Schematic diagram of the integrated ORC.

153 as availability, price, flammability, toxicity, chemical stability [27], and environmental impact  
 154 [27, 30, 32] should be taken into account, as well as safety considerations during handling and  
 155 operation [32]. Regarding environmental aspects, Table 2 highlights indicators such as ozone  
 156 depletion potential (ODP), global warming potential over a 100-year period ( $GWP_{100}$ ) [27, 28,  
 157 30, 31, 33], as well as the NPFA 704 standard for material hazard identification by the National  
 158 Fire Protection Association (NPFA), which provides information on health risks (H), fire hazard  
 159 (F), and instability (I) on a scale from 0 (low hazard) to 4 (very hazardous) [34]. EU guidelines  
 160 and the Montreal Protocol report criteria for WF selection, including a maximum GWP of 150

161 and zero ODP, while also considering the NPFA 704 hazard rating [35]. In the working fluid  
 162 selection process, it is advisable that the condenser pressure be as close to atmospheric pressure as  
 163 possible [28], thus avoiding problems derived from operation, maintenance, and costs of a vacuum  
 164 condenser. For successful selection of organic fluid, a trade-off among all selection criteria is  
 165 necessary, as there is likely no fluid that is suitable in all the aspects discussed earlier [27, 28].

166 Numerous organic working fluids have been suggested in the scientific literature for ORC  
 167 systems driven by high-temperature sources (HTS) [30]. These organic working fluids include  
 168 toluene ( $T_{cond} = 319$  °C), ethylbenzene ( $T_{cond} = 344$  °C), decane ( $T_{cond} = 345$  °C), and cyclohexane  
 169 ( $T_{cond} = 281$  °C) [30, 36, 37], cyclopentane ( $T_{cond} = 239$  °C), cyclohexane ( $T_{cond} = 280$  °C), and  
 170 benzene ( $T_{cond} = 289$  °C) [33]. Temperatures ranging from 250–350 °C are applicable for HTS  
 171 ORC cycles [33]. Accordingly, the exhaust gas temperatures between 330–350 °C of the present  
 172 study are suitable for these ORC systems.

173 Table 2 reports the thermodynamic and environmental properties of the working fluids that  
 174 meet the requirements for application to the ORC system under study, which is driven by an HTS  
 175 between 250–350 °C. All of these properties were retrieved from the RefProp database.

Table 2: Thermodynamic properties of typical organic working fluids proposed for waste heat recovery from high temperature sources [27, 28, 32, 33, 38–41]

Organic fluid	Molar mass	Critical temperature	Critical pressure	Condensation temperature	Condensation pressure	Degradation temperature	Environmental issues <sup>b</sup>				
	kg/kmol	°C	bar	°C @ 1 bar	bar @ 45 °C	°C	GWP <sub>100</sub> <sup>a</sup>	ODP	H	F	I
Cyclopentane	70.13	239	45.83	48.85	0.880	260–280 [42]	4–6	0	1	3	0
Cyclohexane	84.16	280	40.80	80.28	0.300	N/A	4–6	0	1	3	0
Benzene	78.11	289	49.07	79.64	0.299	315 [42]	3–4	0	2	3	0
Toluene	92.14	319	41.26	110.00	0.099	315 [42]	3–4	0	2	3	0
Acetone	58.08	235	46.92	55.69	0.684	> 462 [43, 44]	0.5	0	1	3	0
DMC	90.08	284	49.09	89.69	0.188	N/A	3–4	0	3	3	0
Heptane	100.21	267	27.36	97.95	0.154	260 [42]	3	0	1	3	0
Methylcyclohexane	98.19	299	34.70	100.00	0.151	N/A	2.7	0	1	3	0
Hexane	86.18	235	30.44	68.30	0.451	260–280 [42]	3	0	1	3	0

<sup>a</sup> GWP<sub>100</sub>: Global warming potential in a 100-year period.

<sup>b</sup> Safety information according to the hazard rating system by the National Fire Protection Association (NFPA) of the United States. Each of the health (H), flammability (F) and instability (I) hazards is rated on a scale from 0 (no hazard) to 4 (severe hazard).

176 In addition to the organic working fluid, it is highly recommended to include an additional

177 heat transfer circuit to prevent potential local overheating and chemical instability of the organic  
178 working fluids [30]. Accordingly, a highly stable silicone heat transfer fluid composed of dimethyl  
179 polysiloxane was selected. It has a long lifespan and low fouling potential and is designed to  
180 operate in the liquid phase within the temperature range of  $-40$  to  $398.9$  °C. The heat transfer fluid  
181 is designed to operate at a temperature of  $340$  °C.

## 182 2.2. *Simulation of the integrated organic Rankine cycle unit*

183 Thermoflex®, a product developed by Thermoflow Inc. (Jacksonville, FL, USA), was used  
184 as the simulation software [38]. This program provides simulation and modeling tools for various  
185 types of power plants, ranging from combined cycles and conventional steam cycles to repowering  
186 projects, in addition to a wide variety of renewable energy systems [45–48]. The standout feature  
187 that led to its selection is its extensive library of commercial products, including engine–generator  
188 sets that can be easily customized to fit any other engine from selected manufacturers. Fig. 3  
189 illustrates the schematic used for modeling the diesel generators and generating HSW, as well as  
190 for simulating the ORC unit. The system comprises two fundamental modeling blocks: the diesel  
191 generators and the ORC system. Below are detailed descriptions of the specific features of each  
192 of these subsystems along with their respective modeling approaches.

- 193 • For simulation of diesel generators, the manufacturer’s parameters provided in the technical  
194 manual for the Wärtsilä 12V46F diesel generator shall be followed [26]. The key technical  
195 specifications of these engine–generator sets are summarized in Table 1.
- 196 • The ambient air temperature is assumed to be  $15$  °C.
- 197 • Kim et al. [49] reported a seawater temperature of  $20$  °C for its condenser, while Sellers  
198 et al. [12] considered a higher temperature, specifically  $29$  °C. Another study by Chen et  
199 al. [50] suggested that the temperature throughout the year varies between the two previ-  
200 ously mentioned values. Kosmadakis and Neofytou [51] assumed that the condenser heat  
201 is rejected to a central freshwater cooler with the cooling water entering at a temperature of

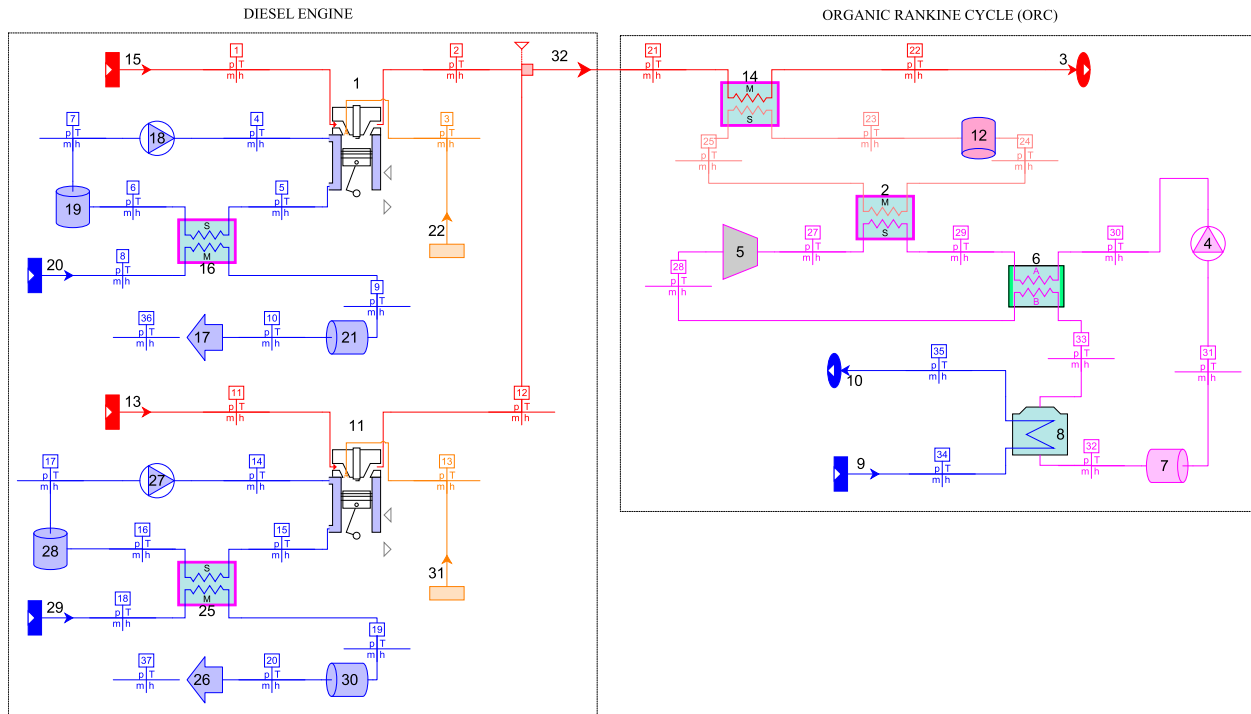


Figure 3: Process simulation flowsheet of the integrated ORC system in Thermoflex.

202 25 °C. Similarly, Lion et al. [52] considered a temperature of 25 °C, which is an average  
 203 temperature and is selected for the simulation.

- 204 • The system is evaluated for a turbine inlet pressure of 20 bar [27, 28, 30]. In the model, the  
 205 turbine inlet temperature ( $TIT$ ) leading to the highest net electrical efficiency is selected for  
 206 each of the evaluated organic fluids.
- 207 • The minimum temperature of the off-gas exiting the HTHX, which transfers heat to the HTF  
 208 circuit supplying the evaporator of the the ORC unit, is set at 120 °C [39].

209 Table 3 presents the operating parameters used in the design of the ORC equipment, as well as  
 210 the assumptions adopted in the heat exchanger equipment for HSW production.

211 Since the overall heat-transfer coefficient for each component in Table 3 is known, the heat  
 212 transfer area of each heat exchanger can be calculated using Eq. (1) [39], which is valid for counter-  
 213 current flows.

Table 3: Design parameters of the ORC bottoming power unit.

Equipment	Performance parameter	Value	Unit	Reference(s)
Expander	Inlet pressure	20	bar	[27, 28]
	Isentropic efficiency	85	%	[27, 53–56]
	Mechanical efficiency	97	%	[27]
High-temperature heat exchanger	Heat transfer efficiency	90	%	[30]
	Minimum pinch point	10	°C	[27, 57]
	Pressure drop	5	%	[53]
	Global heat transfer coefficient	502	W/m <sup>2</sup> K	[58]
Evaporator	Heat transfer efficiency	90	%	[59]
	Minimum pinch point	10	°C	[27, 30, 57]
	Pressure drop	5	%	[53]
	Global heat transfer coefficient	539	W/m <sup>2</sup> K	[58]
Regenerator	Heat transfer efficiency	90	%	[30]
	Minimum pinch point	10	°C	[27, 30, 57]
	Pressure drop	5	%	[53]
	Global heat transfer coefficient	1059	W/m <sup>2</sup> K	[58]
Condenser	Condenser pressure	0.1–1	bar	[27, 28, 30]
	Heat transfer efficiency	95	%	Estimated
	Minimum pinch point	10	°C	[27, 57]
	Pressure drop	2	%	[14]
	Maximum temperature outlet	60	°C	[18]
	Global heat transfer coefficient	833	W/m <sup>2</sup> K	[58]
Pump	Isentropic efficiency	80	%	[14, 27, 30]
	Mechanical efficiency	97	%	[27, 54]
Hot sanitary water heat exchanger	Heat transfer efficiency	85	%	[30]
	Minimum pinch point	10	°C	[27, 57]
	Pressure drop	5	%	[53]
Generator	Electrical efficiency	97	%	[28]

$$\dot{Q} = U A \Delta T_{lm} \quad (1)$$

214 where  $\Delta T_{lm}$  is the logarithmic average temperature difference for each component. This parameter  
215 is determined as follows:

$$\Delta T_{lm} = \frac{(T_{op,in} - T_{ip,out}) - (T_{op,out} - T_{ip,in})}{\ln\left(\frac{T_{op,in} - T_{ip,out}}{T_{op,out} - T_{ip,in}}\right)}. \quad (2)$$

216 where *op* and *ip* refer to the outer and the inner pipe, respectively [39].

217 Table 4 provides a summary of the mass and energy balances for key components of the ORC  
 218 system, together with their corresponding energy efficiencies. Note that  $\dot{Q}_l$  represents the heat flow  
 219 loss associated with each individual component, indicating the energy lost through heat transfer.  
 220 The numbers used for the identification of the different equipment and flow rates are based on the  
 221 process simulation flowsheet of the integrated ORC system in Thermoflex, previously shown in  
 222 Fig. 3.

223 The following equation is used to calculate the thermodynamic efficiency of the ORC:

$$\eta_{ORC} = \frac{\dot{W}_{exp} - \dot{W}_{pump}}{\dot{m}_{wf} \Delta h_{evap}} \quad (3)$$

224 where,  $\eta_{ORC}$  stands for the thermodynamic efficiency of the ORC,  $\dot{W}_{exp}$  represents the output power  
 225 of the expander,  $\dot{W}_{pump}$  denotes the power consumed by the pump,  $\dot{m}_{wf}$  indicates the mass flow rate  
 226 of the working fluid (*wf*), and  $\Delta h_{evap}$  denotes the enthalpy change during the evaporation process.  
 227 Accordingly, Eq. (3) quantifies the efficiency of heat conversion into useful work, considering  
 228 both the power output at the expander and the power input required to drive the working fluid  
 229 through the cycle.

230 The efficiency of the whole bottoming power unit, including the heat transfer fluid (HTF)  
 231 circuit, is calculated as follows:

$$\eta_{htf} = \frac{\dot{W}_{exp} - \dot{W}_{pump}}{\dot{m}_{htf} \Delta h_{htf,HTHX}} \quad (4)$$

232 The net power output ( $\dot{W}_{bottom}$ ) available at the bottom of the ORC unit is obtained through the  
 233 following expression:

Table 4: Mass and energy balance analysis for each component of the ORC system.

N°	Component	Mass balance	Energy balance	Energy efficiency
1	Maritime DG	$\dot{m}_1 + \dot{m}_4 + \dot{m}_3 = \dot{m}_2 + \dot{m}_5$	$\dot{m}_1 h_1 + \dot{m}_3 h_3 + \dot{m}_4 h_4 =$ $+ \dot{m}_2 h_2 + \dot{m}_5 h_5 + \dot{W}_{DG} + \dot{Q}_{l,DG}$	$\eta_{DG} = \frac{\dot{W}_{DG}}{\dot{m}_3 PCI_f}$
16	HSW HX	$\dot{m}_2 + \dot{m}_5 = \dot{m}_6 + \dot{m}_9$	$\dot{m}_5 (h_5 - h_6) =$ $\dot{m}_8 (h_9 - h_8) + \dot{Q}_{l,hs,w,hx}$	$\eta_{hs,w,hx} = \frac{\dot{m}_8 (h_9 - h_8)}{\dot{m}_5 (h_5 - h_6)}$
18	Water cooling pump	$\dot{m}_7 = \dot{m}_4$	$\dot{m}_7 h_7 = \dot{m}_4 h_4 + \dot{W}_{pump} + \dot{Q}_{l,pump}$	$\eta_{pump} = \frac{\dot{m}_4 h_4}{\dot{m}_7 h_7 + \dot{W}_{pump}}$
14	HTF HX	$\dot{m}_{21} + \dot{m}_{23} = \dot{m}_{22} + \dot{m}_{25}$	$\dot{m}_{21} (h_{21} - h_{22}) =$ $\dot{m}_{23} (h_{25} - h_{23}) + \dot{Q}_{l,htf,hx}$	$\eta_{htf,hx} = \frac{\dot{m}_{23} (h_{25} - h_{23})}{\dot{m}_{21} (h_{21} - h_{22})}$
2	Evaporator	$\dot{m}_{25} + \dot{m}_{29} = \dot{m}_{27} + \dot{m}_{23}$	$\dot{m}_{25} (h_{25} - h_{23}) =$ $\dot{m}_{29} (h_{27} - h_{29}) + \dot{Q}_{l,evap}$	$\eta_{evap} = \frac{\dot{m}_{29} (h_{27} - h_{29})}{\dot{m}_{25} (h_{25} - h_{23})}$
5	Expander	$\dot{m}_{27} = \dot{m}_{28}$	$\dot{m}_{27} h_{27} = \dot{m}_{28} h_{28} + \dot{W}_{exp} + \dot{Q}_{l,exp}$	$\eta_{exp} = \frac{\dot{W}_{exp}}{\dot{m}_{27} (h_{27} - h_{28})}$
6	Regenerator	$\dot{m}_{28} + \dot{m}_{30} = \dot{m}_{29} + \dot{m}_{33}$	$\dot{m}_{28} (h_{33} - h_{28}) =$ $\dot{m}_{29} (h_{29} - h_{30}) + \dot{Q}_{l,reg}$	$\eta_{reg} = \frac{\dot{m}_{29} (h_{29} - h_{30})}{\dot{m}_{28} (h_{33} - h_{28})}$
8	Condenser	$\dot{m}_{33} + \dot{m}_{34} = \dot{m}_{32} + \dot{m}_{35}$	$\dot{m}_{34} (h_{35} - h_{34}) =$ $\dot{m}_{33} (h_{33} - h_{32}) + \dot{Q}_{l,cond}$	$\eta_{cond} = \frac{\dot{m}_{33} (h_{33} - h_{32})}{\dot{m}_{34} (h_{35} - h_{34})}$
4	WF pump	$\dot{m}_{31} = \dot{m}_{30}$	$\dot{m}_{30} h_{30} =$ $\dot{m}_{31} h_{31} + \dot{W}_{wf,pump} + \dot{Q}_{l,wf,pump}$	$\eta_{wf,pump} = \frac{\dot{m}_{30} h_{30}}{\dot{m}_{31} h_{31} + \dot{W}_{wf,pump}}$

$$\dot{W}_{bottom} = \eta_{gen} \dot{W}_{exp} - \eta_{em} \dot{W}_{pump} \quad (5)$$

234 where  $\dot{W}_{exp}$  represents the power output of the system, adjusted by the power generation efficiency  
235 of the generator ( $\eta_{gen}$ ). Moreover,  $\dot{W}_{pump}$  denotes the power consumed by the pump, with ( $\eta_{em}$ )  
236 representing its electromechanical efficiency.

237 The efficiency of the bottoming power cycle ( $\eta_{bottom}$ ) is calculated as follows:

$$\eta_{bottom} = \frac{\dot{W}_{bottom}}{\dot{m}_{eg} c_{p,eg} (T_{eg} - T_a)} \quad (6)$$

238 where  $\dot{W}_{bottom}$  refers to the net power output of the ORC unit,  $\dot{m}_{eg}$  denotes the mass flow rate of  
 239 the exhaust gas,  $c_{p,eg}$  represents the specific heat capacity of the exhaust gas,  $T_{eg}$  indicates the  
 240 temperature of the exhaust gas and  $T_a$  represents the ambient temperature.

### 241 2.3. Economic feasibility assessment

242 This section presents the procedure for evaluating the economic performance of the ORC sys-  
 243 tem. The capital cost of the ORC unit includes the purchase equipment cost (PEC) along with addi-  
 244 tional direct fixed-capital investments, indirect fixed-capital investments (IFCI), and other outlays.  
 245 A detailed breakdown of these costs can be found in Section 3.5.

246 The PEC of the ORC unit was determined by aggregating the costs of its individual components  
 247 using the empirical correlations provided in Table 5. The PEC of each heat exchanger in the  
 248 bottoming power unit was calculated based on the required heat transfer area ( $A$ ). Similarly, the  
 249 PECs of the expander, generator, and pump were estimated based on their respective power ratings.

Table 5: Purchase cost correlations of the ORC equipment. All costs are expressed in US dollars.

Equipment	Cost correlation	CEPCI		Sources
		Year	Value	
Condenser	$C_{cond} = 516.62 \times (A_{cond})^{0.85}$	2000	394.1	[57, 60–63]
Evaporator	$C_{evap} = 309.14 \times (A_{evap})^{0.85}$	1997	386.5	[57, 60, 61, 63]
HTF heat exchanger	$C_{HX,htf} = 309.14 \times (A_{HX,htf})^{0.85}$	1997	386.5	[57, 60, 61, 63]
Regenerator	$C_{reg} = 309.14 \times (A_{reg})^{0.85}$	1997	386.5	[57, 60, 61, 63]
Expander	$C_{exp} = 4750 \times (\dot{W}_{exp})^{0.75}$	2010	550.8	[57, 60–63]
Generator	$C_{gen} = 60 \times (\dot{W}_{gen})^{0.95}$	2001	394.3	[60, 63]
Pump	$C_{pump} = 3540 \times (\dot{W}_{pump})^{0.71}$	2011	585.7	[63–65]

250 The economic data presented in Table 5 only reflect the value of the current year. The cost of  
 251 each component is adjusted from the reference year to the current year (2024) using the Chemical  
 252 Engineering Plant Cost Index (CEPCI) according to Eq. (7) [60–63].

$$C_{k,present} = C_{k,reference} \times \frac{CEPCI_{present}}{CEPCI_{reference}} \quad (7)$$

253 where  $C_{k,\text{present}}$  represents the cost of the component  $k$  in the current year,  $C_{k,\text{reference}}$  represents the  
 254 cost of component  $k$  in the reference year,  $\text{CEPCI}_{\text{present}}$  is the Chemical Engineering Plant Cost  
 255 Index for the present year, and  $\text{CEPCI}_{\text{reference}}$  is the Chemical Engineering Plant Cost Index for the  
 256 reference year.

257 The economic feasibility assessment of the ORC system was conducted using standard finan-  
 258 cial appraisal methods. These include the net present value, internal rate of return, profitability  
 259 index, and discounted payback period.

260 The net present value (NPV) represents the difference between the present value of the project's  
 261 future cash flows and the initial investment [66, 67]. This parameter reflects the earnings after  
 262 recovering the initial capital investment (INV). Consequently, if  $\text{NPV} > 0$ , the project is profitable,  
 263 while if  $\text{NPV} < 0$ , it results in a loss.

$$\text{NPV} = \sum_{t=1}^n \frac{\text{NCF}_t}{(1 + \text{WACC})^t} - \text{INV} \quad (8)$$

264 where  $\text{NCF}_t$  is the net cash flow during period  $t$ , WACC is the weighted average capital cost used  
 265 as the discount rate, INV is the initial capital investment, and  $n$  represents the project lifetime in  
 266 years.

267 The time required to recover the initial investment, accounting for the annual discount rate,  
 268 is known as the discounted payback period (DPB). This metric is calculated using Eq. (9), which  
 269 assumes equal cash flows, making it applicable only for scenarios with constant cash inflows.  
 270 Therefore, an average annual cash flow is used in this calculation.

$$\text{DPB} = \frac{\log \left( \frac{1}{1 - \frac{\text{INV} \times \text{WACC}}{\frac{\sum_{t=1}^n \text{NCF}_t}{n}}} \right)}{\log(1 + \text{WACC})} \quad (9)$$

271 The internal rate of return (IRR) refers to the discount rate that results in a zero NPV for the

272 project, indicating the maximum discount rate for which the investment breaks even.

$$\text{NPV} = \sum_{t=1}^n \frac{\text{NCF}_t}{(1 + \text{IRR})^t} - \text{INV} = 0 \quad (10)$$

273 Finally, the profitability index (PI) is defined as the ratio of the net present value to the initial  
274 investment [67]. A PI value greater than unity indicates that the project is profitable.

$$\text{PI} = \frac{\text{NPV}}{\text{INV}} \quad (11)$$

### 275 3. Results and discussion

276 This section presents a detailed analysis of the integrated system's performance, including a  
277 comparison of various organic working fluids in terms of efficiency and thermodynamic behavior.  
278 A Sankey diagram is used to illustrate energy flows, losses, and efficiencies. Additionally, an  
279 off-design analysis is conducted to evaluate system performance under real operating conditions.  
280 Finally, an economic assessment is carried out to determine the system's feasibility and cost-  
281 effectiveness.

#### 282 3.1. Integrated organic Rankine cycle and selection of the working fluid

283 Fig. 4 compares the bottoming efficiency ( $\eta_{bottom}$ ) and the condensation temperature ( $T_{cond}$ ) of  
284 the ORC unit for various organic working fluids as functions of the condenser pressure. The flu-  
285 ids examined include cyclopentane, cyclohexane, benzene, toluene, acetone, dimethyl carbonate  
286 (DMC), heptane, methylcyclohexane, and hexane. Each plot shows multiple curves corresponding  
287 to different turbine inlet temperatures ( $TIT$ ). In particular, acetone and cyclopentane demonstrate  
288 the capability to achieve the lowest condensation temperatures without significant penalties in ef-  
289 ficiency, even at higher condenser pressures. Under ambient pressure conditions for operating  
290 the condenser, the bottoming efficiency with these working fluids is in the range of 9–10%. This  
291 makes them particularly advantageous because of their ability to operate the condenser at near

292 ambient pressure to avoid air leakage, which may adversely affect the ORC unit if the condenser  
293 pressure is excessively low. Accordingly, trade-offs must be carefully considered when selecting a  
294 working fluid for specific thermodynamic cycles. Although other fluids may reach higher efficien-  
295 cies under low-pressure conditions, they also suffer more pronounced efficiency reductions with  
296 increasing condenser pressure and exhibit higher minimum condensation temperatures. Benzene,  
297 for example, can achieve a comparable bottoming efficiency under ambient pressure, but its con-  
298 densation temperature is significantly higher at 79.6 °C, compared to cyclopentane (48.8 °C) and  
299 acetone (55.7 °C).

300 Table 6 presents a comparative analysis of the efficiencies of the ORC using cyclopentane and  
301 acetone as working fluids under different engine load conditions (85% and 100%). The results  
302 indicate that the thermodynamic efficiency ( $\eta_{\text{ORC}}$ ) is slightly higher for cyclopentane, with values  
303 of 20.02% and 20.30% for 85% and 100% engine load, respectively, compared to acetone, which  
304 has values of 18.73% and 19.09% under the same conditions. Similarly, the efficiency at the  
305 HTHX ( $\eta_{\text{htf}}$ ) follows the same trend, with cyclopentane showing values of 18.02% and 18.27%,  
306 whereas acetone achieves 16.85% and 17.18% for the respective engine loads.

307 Regarding the net electrical efficiency ( $\eta_{\text{bottom}}$ ), cyclopentane again demonstrates a slight ad-  
308 vantage over acetone. For an engine load of 85%, cyclopentane achieves an efficiency of 9.04%,  
309 and for a 100% load, it reaches 9.65%. In comparison, acetone has efficiencies of 8.45% and  
310 9.20% under the same conditions. These findings suggest that cyclopentane is a marginally more  
311 efficient working fluid than acetone in terms of converting thermal energy to electrical energy,  
312 potentially making it a better choice for specific applications in ORC units under the evaluated  
313 operating conditions.

314 The temperature-specific entropy ( $T-s$ ) diagram of the two analyzed fluids for the offshore  
315 diesel generators operating at 100% load is presented in Fig. 5. The  $T-s$  diagram of the ORC with  
316 cyclopentane as WF illustrates the operation between temperatures of 45 °C and 220 °C, while  
317 the  $T-s$  diagram of acetone operates at a higher  $TIT$  of 225 °C. In both cycles, the first stage

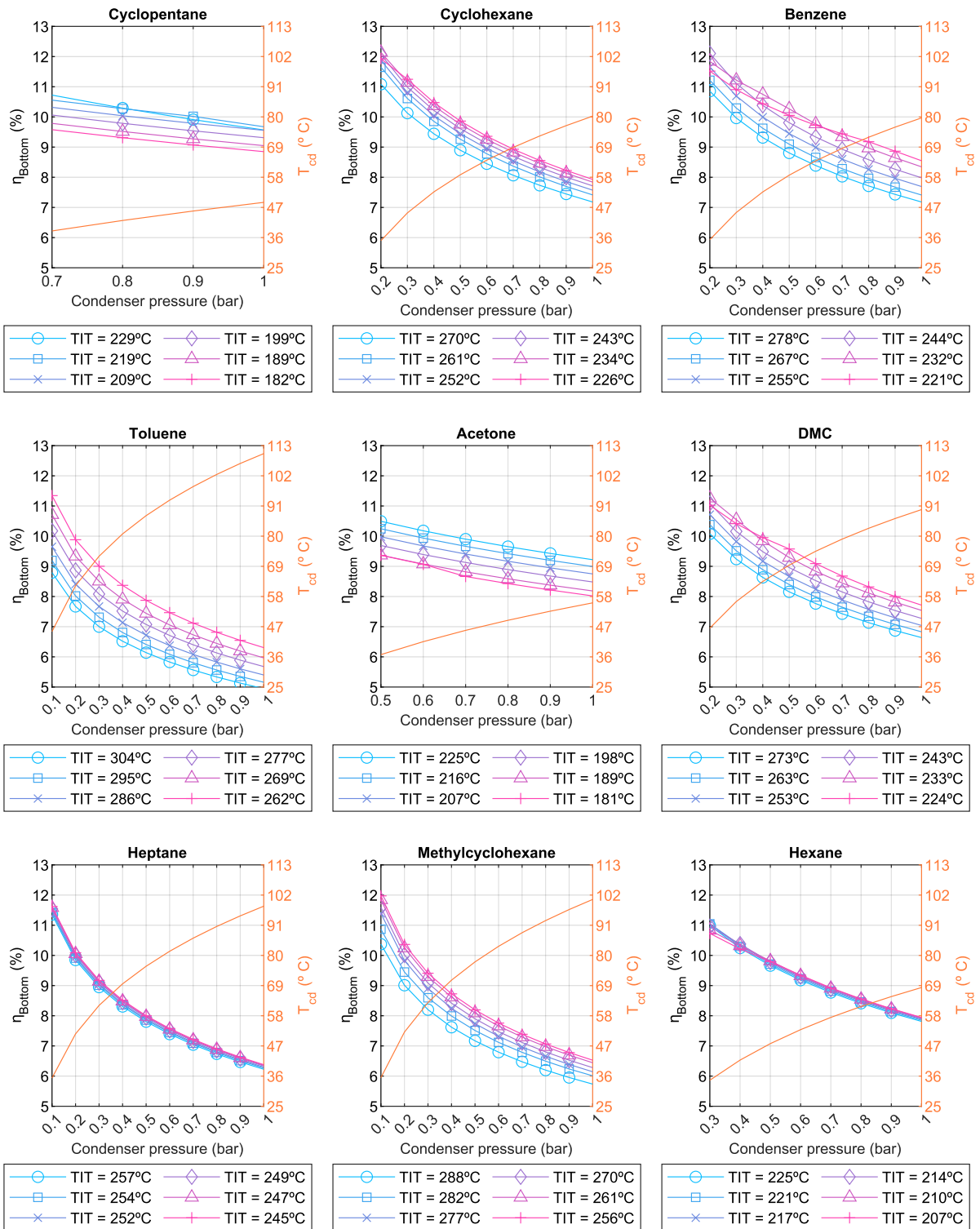


Figure 4: ORC system performances for the different organic liquids tested at different condensation pressures.

Table 6: Performance parameters of the organic Rankine cycle under design conditions for the working fluids selected.

Performance parameter	Organic working fluid				Unit
	Cyclopentane		Acetone		
	85% engine load	100% engine load	85% engine load	100% engine load	
Exhaust gas temperature ( $T_{eg}$ )	330	364	330	364	°C
Exhaust gas flow rate ( $\dot{m}_{eg}$ )	44.88	51.90	44.88	51.90	°C
Turbine inlet temperature ( $TIT$ )	214	220	218	225	°C
Condensation temperature ( $T_{cond}$ )	48.85	48.85	55.69	55.69	°C
Condensation pressure ( $p_{cond}$ )	1	1	1	1	bar
Pressure in evaporator ( $p_{evap}$ )	20	20	20	20	bar
Off-gas temperature ( $T_{og}$ )	120	123.6	120	120	°C
HTF mass flow rate ( $\dot{m}_{htf}$ )	22.09	25.89	22.22	24.88	kg/s
WF mass flow rate ( $\dot{m}_{wf}$ )	15.41	20.33	12.41	16.63	kg/s
Sea water mass flow rate ( $\dot{m}_{sw}$ )	102.7	188.4	70.97	95.05	kg/s
UA HTF HX	895.2	1028.9	894.3	705.2	kW/°C
UA evaporator	414.1	404.6	288.5	500.1	kW/°C
UA regenerator	112.3	112.3	63.3	63.3	kW/°C
UA condenser	364.7	536	325.5	435.9	kW/°C
Pump power consumption ( $\dot{W}_{pump}$ )	89.08	117.7	68.67	92.0	kW
Gross electric power ( $\dot{W}_{bottom, gross}$ )	1813.48	2322.10	1598.17	2195.43	kW
Net electric power ( $\dot{W}_{bottom, net}$ )	1724.40	2204.40	1529.5	2103.43	kW
Thermodynamic efficiency ( $\eta_{ORC}$ )	20.02	20.30	18.73	19.09	%
HTF efficiency ( $\eta_{htf}$ )	18.02	18.27	16.85	17.18	%
Net electrical efficiency ( $\eta_{bottom}$ )	9.04	9.65	8.45	9.20	%

318 is compression, where the pressure of the working fluid (WF) increases, causing a slight rise in  
319 temperature. The WF then undergoes heating and evaporation. During this stage, its temperature  
320 increases in the regenerator, and it evaporates by transferring heat from a high-temperature heat  
321 transfer fluid (HTF), which significantly raises its entropy. When the working fluid reaches the  
322 desired turbine inlet temperature ( $TIT$ ), it expands in the turbine, doing useful work and further  
323 increasing its entropy. After leaving the expander, the WF passes through the regenerator to re-  
324 cover some residual heat. Finally, in the condensation stage, the WF releases heat to the cooling  
325 water (CW) and condenses at 45 °C. It is noteworthy that assuming a condensation temperature  
326 of 45 °C is a rather conservative approach, as it provides a safety margin that ensures a minimum  
327 pinch point temperature difference of at least 10 °C if the surface seawater temperature is close to  
328 30 °C.

329 Despite its slightly lower efficiency, acetone is preferable to cyclopentane due to its lower cost  
330 and global warming potential, with similar safety aspects to those of cyclopentane, as outlined in

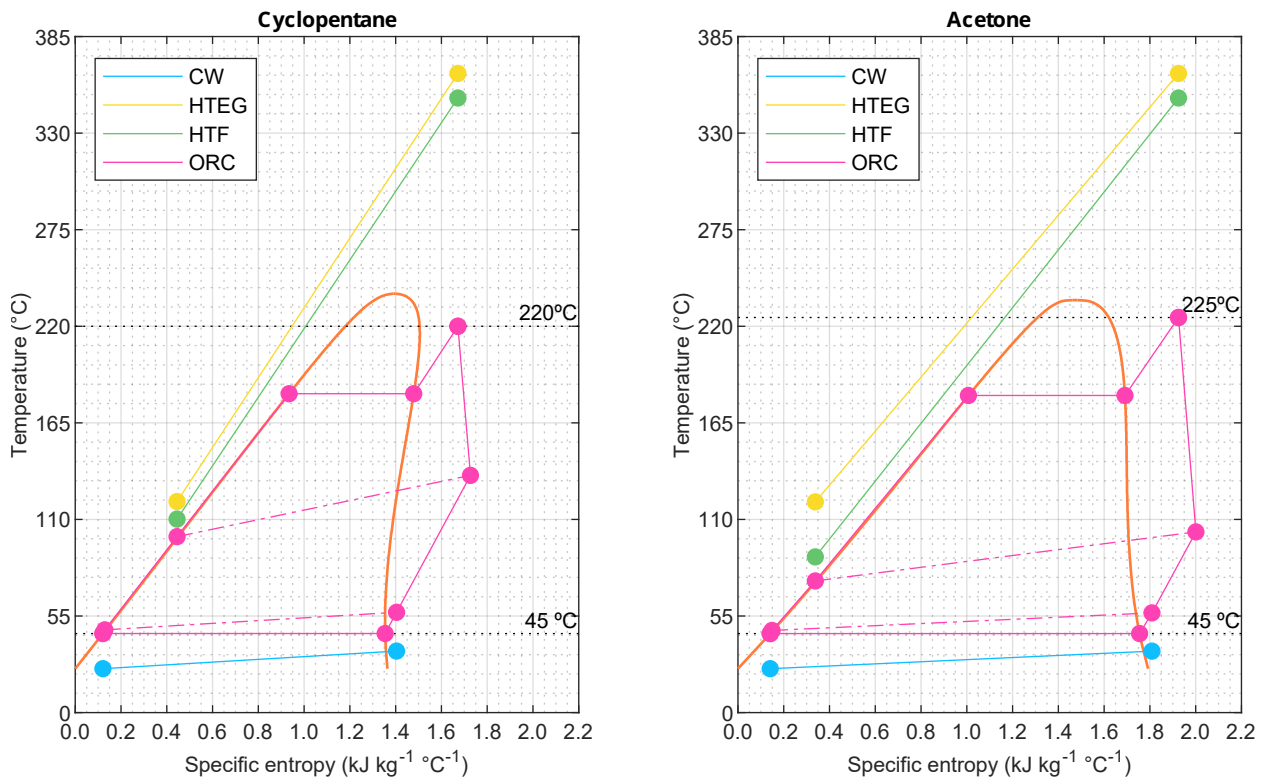


Figure 5:  $T$ - $s$  diagrams of the pre-selected organic working fluids.

331 Table 2. Pantaleo et al. [39] compared the performance of ORC power units in waste-heat recovery  
 332 (WHR) applications for a broad range of working fluids. Their findings revealed that acetone  
 333 consistently yielded the highest optimized power output, with the exception of the single-stage  
 334 screw expander, where cyclopentane performed comparably. Additionally, the study assessed  
 335 exergy losses, determining that the optimal fluid minimizes exergy losses in both the condenser  
 336 and evaporator. Acetone was again the best option, as it resulted in the lowest overall exergy losses  
 337 in the heat exchangers.

338 To further validate the decision to select acetone as the working fluid, the associated expo-  
 339 sure risks in maritime environments were assessed. Acetone is preferred over cyclopentane due  
 340 to its higher water solubility, which facilitates rapid dilution and mitigates the risks associated  
 341 with surface contamination and bioaccumulation [68]. Moreover, acetone is readily biodegradable  
 342 by microorganisms in both soil and aquatic environments, further supporting its environmental

343 compatibility [68]. By contrast, cyclopentane is largely insoluble in water [69], leading to the for-  
344 mation of persistent surface layers that can detrimentally affect marine ecosystems. Cyclopentane  
345 is toxic to aquatic organisms, and it is strongly advised not to let the chemical enter the marine  
346 environment [70].

347 On the other hand, acetone exhibits a higher autoignition temperature (465 °C) [71], com-  
348 pared to that of cyclopentane (361 °C) [69], making it less susceptible to spontaneous combustion  
349 in maritime storage and transport conditions. Even though both acetone and cyclopentane are  
350 highly flammable, acetone has a broader flammable range in air (2.6%–12.8%) [71], in contrast to  
351 cyclopentane's narrower range (1.1%–8.7%) [69].

352 Finally, acetone stands out as one of the most widely used working fluids in ORC system stud-  
353 ies [72–77], due to its favorable chemical properties, including thermal stability, low molecular  
354 weight, and suitable critical point constants [72]. Notably, Meziane et al. [43] reported a degrada-  
355 tion temperature of 527 °C. Additionally, Davoud et al. [44] found that acetone degrades within  
356 a temperature range of 500–600 °C, decreasing to 462 °C with prolonged residence times, which  
357 remains well above typical operating conditions.

### 358 3.2. Sankey diagram

359 Fig. 6 shows a detailed Sankey diagram of the system evaluated in the case of full load opera-  
360 tion. The diagram shows the main outgoing power flows from both diesel generators.

361 Approximately 45.3% of the energy released from the combustion of the fuel is converted into  
362 shaft power. The generator, with an efficiency of 98%, achieves a net electricity generation of  
363 14,400 kWh, with 0.86% of the input energy flow constituting generator losses. Accordingly, the  
364 gross electrical efficiency of the diesel generator is 44.4%. From the cooling circuit, an output  
365 power of 1,824 kW (5.6% of the input power) is obtained, resulting in 1,550.4 kW of HSW in a  
366 heat exchanger, which is equivalent to 4.8% of the input energy flow. The remaining input power  
367 of the generator is distributed as follows: 9.6% to a high-temperature charge air heat circuit, 4.7%  
368 to a low-temperature charge air heat circuit, 4.5% to a lubricating oil circuit, and 1.4% to radiation

369 losses. Additionally, 28.9% of the fuel energy is transferred to the exhaust gases. The same energy  
370 flow distribution is applicable to the second diesel generator.

371 In the mixer, the two energy flows from the exhaust gases of the diesel generators are combined.  
372 This amounts to a total input energy flow of 18,732 kW to the integrated ORC system. This heat  
373 flow is considered as the reference value for evaluating the ORC system. The exhaust gases pass  
374 through the high-temperature heat exchanger (HTHX), transferring 65.4% of their energy to the  
375 heat transfer fluid. The remainder consists of losses in the HTHX (7.2%) and waste heat remaining  
376 in the exhaust gases (27.4%), as they leave the system at a temperature of 120 °C. Following this,  
377 the heat transfer fluid transfers the majority of its energy to acetone in the evaporator (58%), with  
378 the remaining 7.4% representing losses from the equipment. Moreover, the regenerator serves as  
379 a loop to enhance the system's energy before the working fluid enters the expander, transferring  
380 5.9% of the energy from the fluid leaving the expander to the fluid exiting the pump. However, this  
381 process also entails losses within the regenerator, amounting to 0.65%. Consequently, the energy  
382 flow recovered from the organic fluid in the regenerator is 6.55%. In the condenser, 43.9% of the  
383 energy contained in the exhaust gases is transferred to the cooling seawater, with 2.3% representing  
384 heat losses to the environment. The expander extracts 2334.3 kW from the working fluid (12.5%),  
385 with mechanical losses and generator losses representing 0.37% and 0.36% of the input energy  
386 flow in the exhaust gas, respectively. Finally, the ORC system provides a gross electrical power  
387 output of 2195.4 kW (11.7%). The operation of the pump requires a power consumption of 91.97  
388 kW. In the ORC system, this contributes 88.8 kW to increasing the enthalpy of the cold fluid before  
389 entering the regenerator, as a result of the pressure increase from 1 to 20 bar. Finally, the system  
390 produces a net AC power output of 30.9 MW.

391 When considering the input energy flow of both diesel generators as 100%, the system adds  
392 an additional 3.4% to the electrical power output, reaching a net electrical efficiency of the whole  
393 system ( $\eta_{e,net}$ ) equal to 48.7%. This represents a reasonably high performance, since nearly half  
394 of the input energy flow to the system can be converted into electric power to supply the loads

395 and the ship's propulsion system. Additionally, 3.1 MW of waste heat can be recovered through  
396 jacket cooling water heat exchangers for the production of HSW (4.8% of the input energy flow).  
397 Therefore, the CHP system allows reaching a net overall efficiency ( $\eta_{\text{CHP,net}}$ ) of 53.5%.

398 For comparison, Herrera et al. [78] reported a thermodynamic efficiency ( $\eta_{\text{ORC}}$ ) of approxi-  
399 mately 22.5% for an ORC cycle using acetone, which is slightly higher than the thermodynamic  
400 efficiency of 19.1% achieved in the present study. This slight difference is attributed to the higher  
401 evaporator pressure of 24 bar adopted in the study by Herrera et al. [78] compared to the maximum  
402 pressure of 20 bar used in this work. By contrast, Pantaleo et al. [39] reported a thermodynamic  
403 efficiency of 15% under operating conditions of 24.9 bar and a condensation pressure of 1.13 bar.  
404 Furthermore, the expander efficiency in that study was 64%. Despite this, the expander efficiency  
405 of 85% used here is frequently cited in the literature. Although Choudhary et al. [79] assumed a  
406 higher isentropic efficiency of 90%, most authors typically report lower isentropic efficiencies of  
407 around 85%, [27, 53–56].

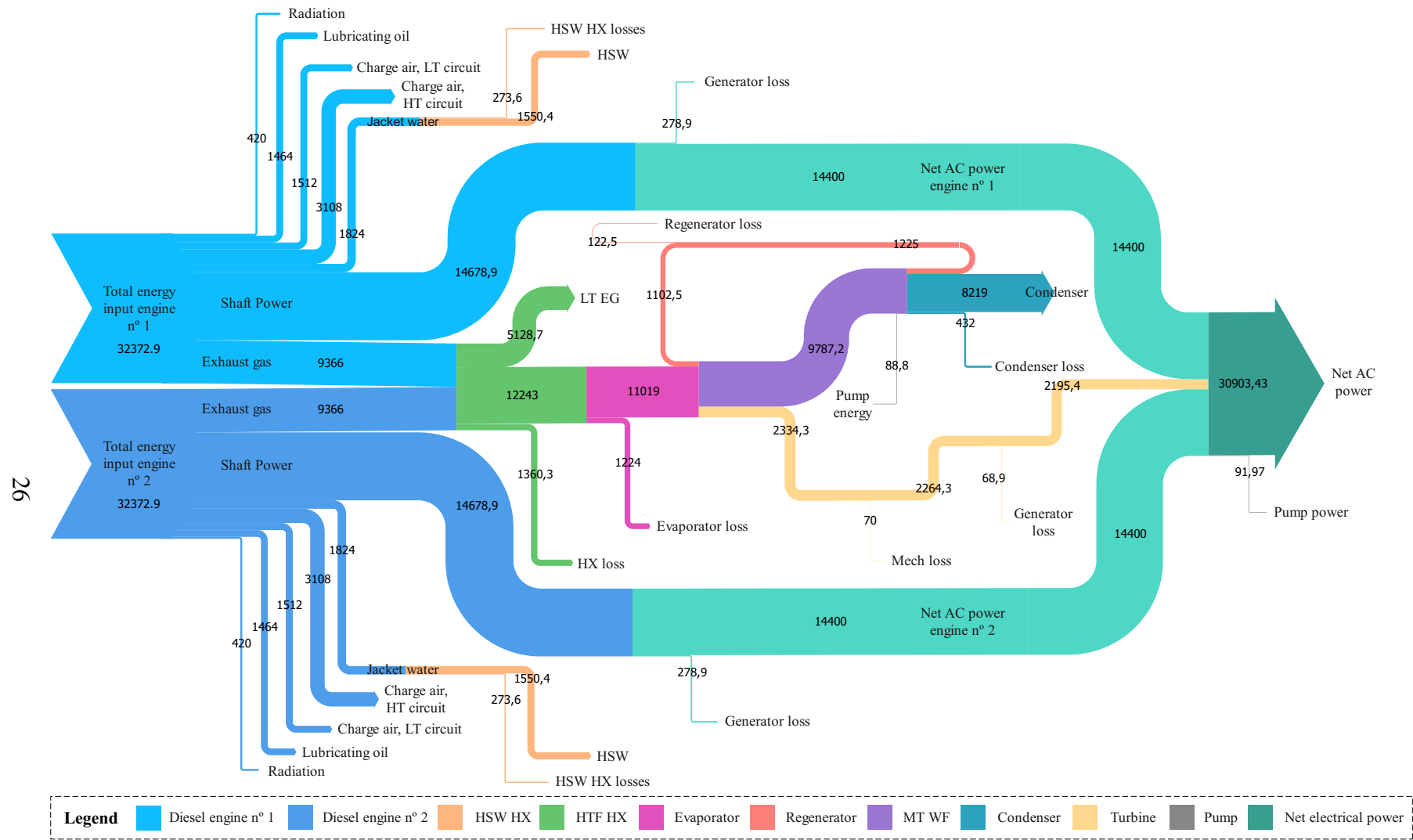


Figure 6: Sankey diagram of the marine diesel engine and ORC system under full load operation.

### 408 3.3. Off-design performance of the integrated organic Rankine cycle unit

409 In order to evaluate the behavior of the system under real operating conditions, an ORC unit  
410 designed to operate with acetone and optimized for 85% load of the port engines is analyzed in this  
411 section. The term “off-design” refers to operating conditions that do not match the optimal param-  
412 eters established during the system’s design [80–82]. This concept is key to understanding how  
413 the ORC responds when operating outside its ideal range, which can affect its efficiency, perfor-  
414 mance, and reliability. Analyzing these off-design conditions is essential to optimize performance  
415 in various operational scenarios and to ensure the system’s safety and adaptability to changes in  
416 the environment or load.

417 Fig. 7 provides a comprehensive analysis of the performance of the diesel generator and ORC  
418 bottoming unit under different off-design conditions.

419 Fig. 7a) illustrates the relationship between the exhaust gas energy flow and the net power  
420 output of the ORC system and the diesel generator. For the diesel generator, a linear trend is  
421 evident, indicating a direct increase in power output with rising exhaust gas energy flow. However,  
422 the net power output of the ORC system follows a less straightforward trend.

423 Fig. 7b) shows various efficiencies of the bottoming power unit as a function of the exhaust  
424 gas energy flow. The efficiency of the HTHX ( $\eta_{htf}$ ) remains relatively stable around 18.5–19%,  
425 indicating consistent performance of the HTHX at varying loads. By contrast, the efficiency of  
426 the bottoming power unit ( $\eta_{bottom}$ ) exhibits a slightly higher increase with the rise in exhaust gas  
427 energy flow, reaching values close to 8%.

428 Fig. 7c) presents the minimum specific fuel oil consumption (SFOC) of multiple diesel gen-  
429 erators operating simultaneously for varying power loads. Variations in SFOC are observed with  
430 changes in generator power, displaying a stepped behavior that reflects different operational zones  
431 depending on the number of generators in operation. As the number of simultaneously operating  
432 diesel generators increases, the total power delivered by the diesel generators rises, and the SFOC  
433 shows a slight increasing trend.

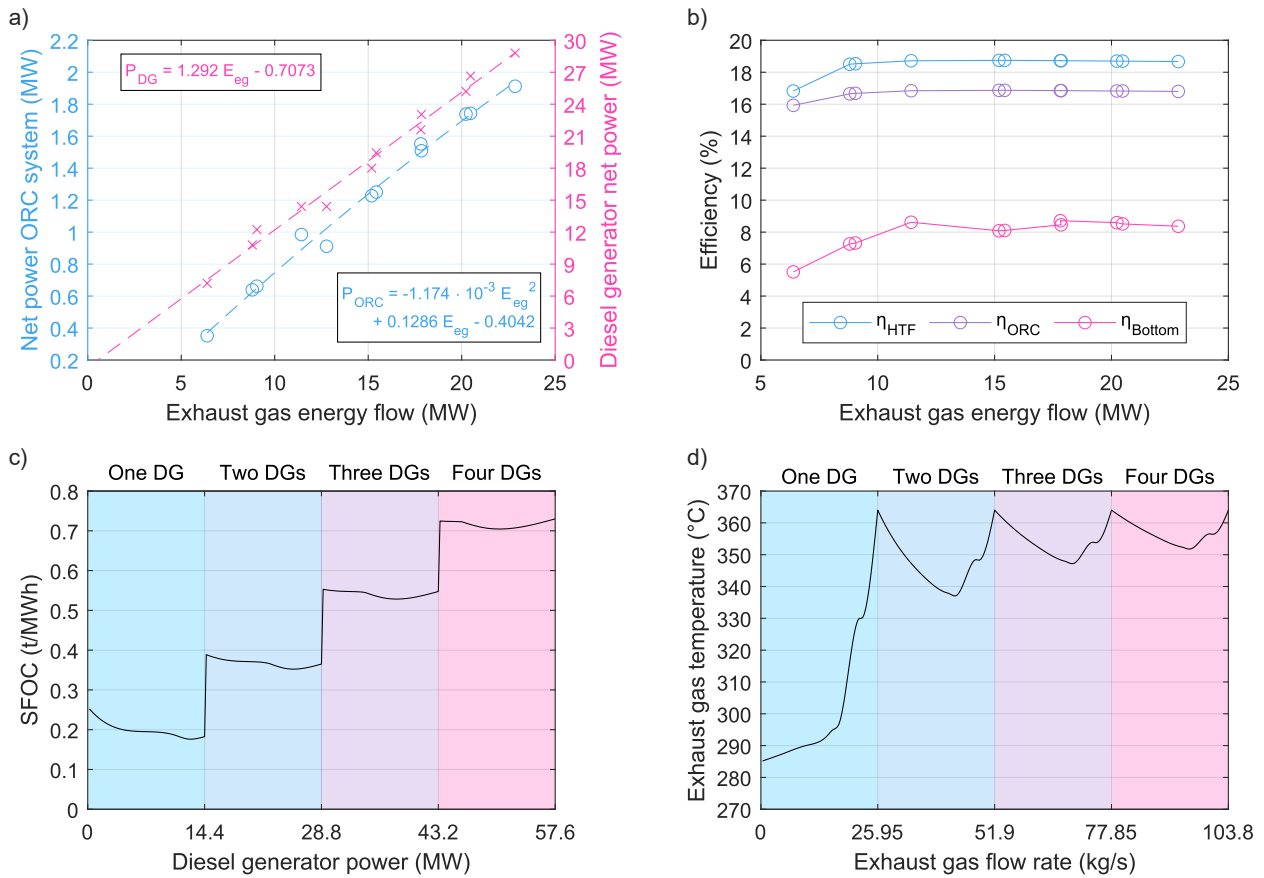


Figure 7: *a)* Net power of the ORC system and diesel generators in off-design mode as a function of the exhaust gas energy flow, *b)* ORC system efficiencies in off-design mode as a function of the exhaust gas energy flow, *c)* Minimum SFOC curve of various diesel generators (DGs) operating simultaneously for different powers served, and *d)* Exhaust gas temperature and flow rate of various diesel generators (DGs) operating simultaneously.

434 Finally, *7d)* represents the exhaust gas temperature and flow rate of various diesel generators  
 435 (DGs) operating simultaneously. Temperature variations in the exhaust gases are observed when  
 436 operating with one or a combination of engines. When using a single engine up to 50% load, the  
 437 temperature remains below 297 °C. However, as the diesel generator load increases beyond 50%,  
 438 the exhaust temperature progressively rises, reaching 364 °C at full load. Operating multiple en-  
 439 gines simultaneously results in a higher exhaust gas flow rate, which in turn stabilizes the exhaust  
 440 gas temperature. The increased flow rate provides more energy, leading to enhanced performance  
 441 of the ORC system and improving overall system efficiency. By contrast, when operating with a  
 442 single engine, load variations have a greater influence on the exhaust gas temperature. However,

443 with the simultaneous operation of several diesel generators, the exhaust gas temperature becomes  
444 more stable, and small load variations have a reduced impact on the exhaust gas temperature.

#### 445 *3.4. Route performance*

446 Baldi et al. [83] conducted a detailed analysis of the energy performance of a cruise ship operat-  
447 ing in the Baltic Sea using operational data measured over one year. The ship's propulsion system  
448 includes two propulsion lines, each with two four-stroke Wärtsilä diesel engines, and propulsion  
449 accounts for 70% of annual energy consumption. However, the ship's maximum speed is rarely  
450 utilized, and most of the time, only one or two engines are operating simultaneously [83]. For  
451 this reason, in this work the ORC system has been evaluated with acetone as working fluid at 85%  
452 load of the port diesel generators. Baldi et al. [83] reported that electricity and heat demands are  
453 approximately 10% and 20% of the total energy consumption, respectively, supporting systems  
454 such as high-temperature heat recovery, steam systems, auxiliary boilers, and various electrical  
455 consumers. The route data provided by Baldi et al. [83] were adjusted to match the system's nom-  
456 inal power for optimization, aiming to minimize diesel consumption and maximize ORC usage to  
457 meet electrical demands. The operation of diesel generators and the ORC system was simulated  
458 using the results obtained from the off-design study (Section 3.3).

459 Fig. 8 shows the distribution of instantaneous power demand and generation on a ship over  
460 four typical days spanning different seasons, detailing the contributions of the port and starboard  
461 diesel generators, as well as the ORC system.

462 Over the four days, power demand varies significantly, influencing the operation of port and  
463 starboard diesel generators and the ORC system. On Day 1, demand fluctuates between 5 MW  
464 and 20 MW, managed by port diesel generators, with the ORC system contributing steadily but  
465 shutting down when the engine load drops below 50% between 16h and 20h. Day 2 starts with  
466 high demand (45–50 MW), which drops to 5 MW and stabilizes at 10–15 MW, leading both port  
467 and starboard generators to adjust accordingly. The ORC system operates consistently until 11h  
468 but shuts down until 18h due to low engine load. Day 3 sees an initial demand of 10 MW, peaking

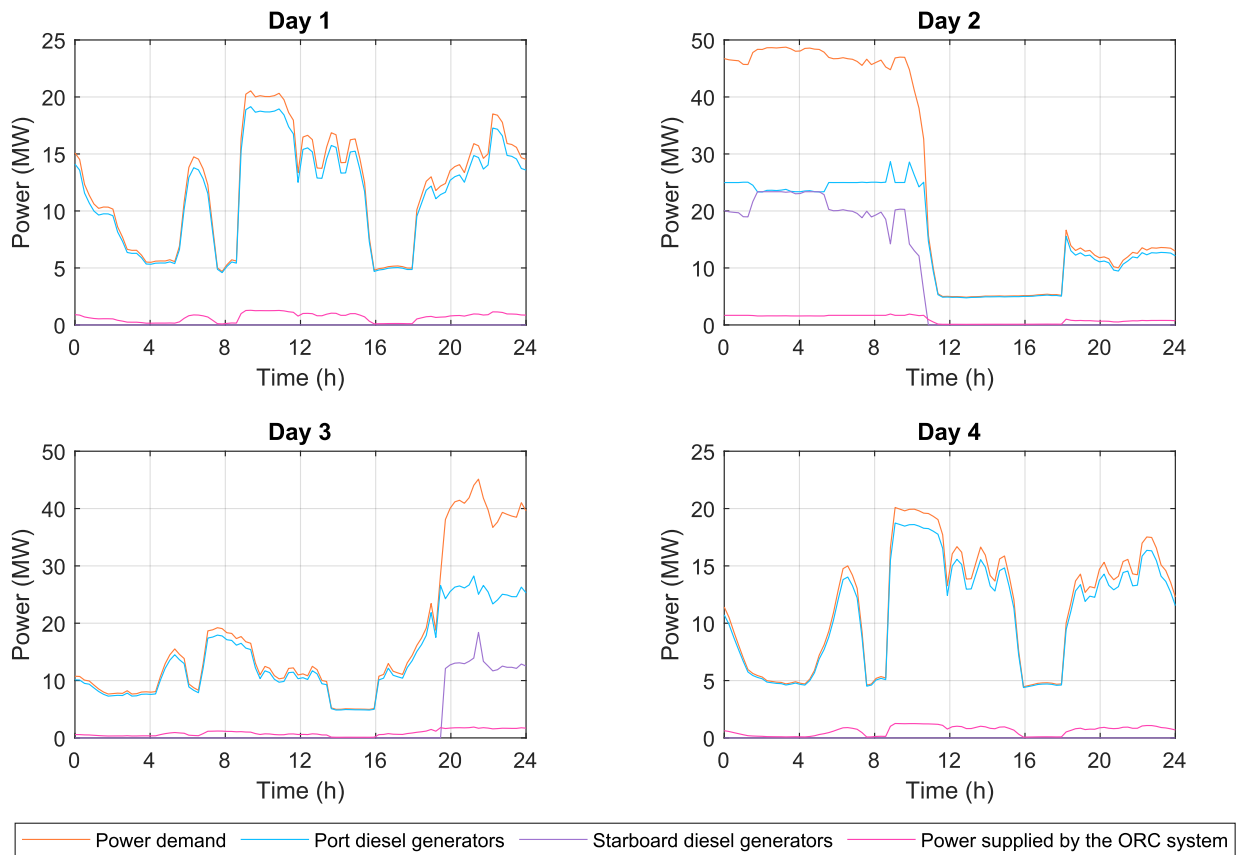


Figure 8: Route performance on various typical days.

469 at 45 MW around 20h, prompting the activation of starboard generators as demand exceeds 30  
 470 MW, while the ORC system maintains a low, constant contribution. On Day 4, demand fluctuates  
 471 between 5 MW and 20 MW with multiple peaks, managed by port generators, and the ORC system  
 472 provides minimal output, shutting down when the engine load falls below 50%.

473 Table 7 presents the cumulative data for each of the days analyzed. In particular, the analysis  
 474 indicates an average daily reduction in diesel consumption by 1.4 tonnes, resulting in a daily  
 475 decrease of 4.4 tonnes of CO<sub>2</sub> emissions, considering that the fuel contains 86.6% carbon [84].  
 476 Extrapolating these data over an annual period, the implementation of the ORC system would  
 477 reduce diesel consumption and CO<sub>2</sub> emissions by 18.5%. These values are comparable to those  
 478 presented by Bouman et al. [85] and Baldasso et al. [86], who suggested that the installation of  
 479 WHR units on board vessels could lead to a reduction in CO<sub>2</sub> emissions in the range of 1% to

480 20%.

Table 7: Total energy generation, diesel consumption and CO<sub>2</sub> emissions of the vessel by route.

Case	Component	Total energy generated (MWh)				Diesel consumption (t)				CO <sub>2</sub> emissions (t)			
		Day 1	Day 2	Day 3	Day 4	Day 1	Day 2	Day 3	Day 4	Day 1	Day 2	Day 3	Day 4
1	Port diesel generators	274.43	376.45	328.34	261.54	5.84	6.48	6.07	5.67	18.57	20.56	19.27	18.03
	Starboard diesel generators	0	216.00	58.43	0								
	ORC System	16.15	23.43	20.07	15.04	0	0	0	0	0	0	0	0
2	Base case (4xWärtsillä 12V46F)	291.97	616.64	408.22	277.92	6.27	10.16	7.02	6.06	19.91	32.26	22.27	19.23

### 481 3.5. Economic feasibility assessment

482 The capital cost of the ORC unit was determined using the correlations previously reported  
 483 in Table 5, adjusted using the CEPCI to the current year. Accordingly, the PEC of the ORC  
 484 in 2024 is estimated to be approximately \$1490/kW<sub>e</sub>. To provide context, Pantaleo et al. [39]  
 485 conducted a thermoeconomic optimization study on small-scale ORC systems designed for WHR.  
 486 They evaluated 18 organic working fluids and found power capital costs in the range of \$2000–  
 487 5000/kW<sub>e</sub>. It is noteworthy that the power capital cost of an ORC unit generally decreases with an  
 488 increase in electrical power output [87]. Accordingly, for systems with relatively high electrical  
 489 power outputs (>1 MW<sub>e</sub>), the power capital cost is typically lower than €3000/kW<sub>e</sub> [87]. Girgin  
 490 et al. [88] also reported that the cost of various ORC systems from different manufacturers for  
 491 naval applications ranges from \$1800 to \$2857 per kW.

#### 492 3.5.1. Baseline assessment

493 The following assumptions have been made for the techno-economic assessment of the base-  
 494 line scenario.

- 495 • Based on the findings reported in Table 5, average daily savings of 2.5 tonnes of diesel fuel  
 496 are considered.
- 497 • The density of marine diesel fuel is estimated at 900 kg/m<sup>3</sup> [93].
- 498 • An average diesel price of \$0.85 per liter is assumed, based on the latest data (between 2020  
 499 and 2024) from the ANAVE (Spanish Shipping Association) [94].

Table 8: Cost breakdown of installing an ORC bottoming unit (1.6 MW<sub>e</sub>) to recover waste heat from Wärtsilä 12V46F diesel generators for additional power generation.

Cost breakdown	Percentage range	Applied percentage	Cost estimate ( \$ )
<b>Fixed-capital investment (FCI)</b>			<b>\$ 6,244,900</b>
<b>Direct fixed-capital investment (DFCI)</b>			<b>\$ 5,027,300</b>
Purchased-equipment cost (PEC)	N/A	N/A	\$2,382,600
Purchased-equipment installation	45% of PEC [89] 30% of PEC [58] 50% of PEC [90]	40% of PEC	\$ 953,050
Piping	31% of PEC [89] 20% of PEC [58] 30% of PEC [90] 9% of PEC [91]	27% of PEC	\$643,310
Instrumentation and control	10% of PEC [89] 10% of PEC [58] 20% of PEC [90] 5% of PEC [91]	12% of PEC	\$285,920
Electrical equipment and materials	10% of PEC [89] 10% of PEC [58]	10% of PEC	\$238,260
Structural and architectural work	10% of PEC [89] 15% of PEC [58]	12% of PEC	\$285,920
Service facilities	10% of PEC [89]	10% of PEC	\$238,260
<b>Indirect fixed-capital investment (IFCI)</b>			<b>\$ 1,217,500</b>
Engineering and supervision	30% of PEC [89] 25% of PEC [58] 50% of PEC [90]	30% of PEC	\$714,790
Construction costs (including contractor's profit)	10% of DFCI [89]	10% of DFCI	\$502,730
<b>Other outlays</b>			<b>\$ 958,820</b>
Contingencies	10% of FCI [89] 20% of PEC [58]	20% of PEC	\$476,530
Startup costs and working capital	10% of FCI [39, 89] 10% of PEC [92] 20% of PEC [58]	15% OF PEC	\$357,390
Legal costs	2% of FCI [89]	2% of FCI	\$124,900
<b>Total capital investment</b>			<b>\$ 7,203,700</b>

- 500 • Direct and indirect fixed-capital investment costs as a percentage of the PEC are provided in  
501 the literature [58, 89, 90]. Table 8 shows a breakdown of all costs associated with the project.  
502 The installation of an ORC unit of 1.6 MW<sub>e</sub> requires a capital investment of \$7,203,700,  
503 which constitutes an approximate capital cost value of \$4,500/kW<sub>e</sub>.

- 504 • For the operational and maintenance (O&M) costs of the ORC system equipment, a conser-  
505 vative estimate of 20% of the total PEC price is assumed [57]. In related studies, Gomaa  
506 et al. [91] suggested O&M values over the project’s lifespan, with 4% for heat exchangers  
507 and 2% for the pump and expander, based on the PEC price. Additionally, Pallis et al. [21]  
508 indicated an annual O&M cost of 2% of the PEC.
- 509 • For vessel operation, a shipping time of 8640 hours per year (approximately 360 days) is  
510 assumed. For comparison, Lion et al. [52] reported 340 days of operation, typical for a  
511 chemical tanker making 8 voyages per year from Dubai to Hamburg.
- 512 • The project lifespan is assumed to be 25 years [86, 95]. A relatively lower lifespan of 20  
513 years has been assumed in related works [21, 96, 97].
- 514 • A rather conservative discount rate (interest rate) of 8% has been assumed [21]. For context,  
515 lower discount rates of 5% were considered in related studies by Shu et al. [98], Wang et al.  
516 [99] and Konur et al. [96]; while a discount rate of 6% was assumed by Baldasso et al. [95].  
517 By contrast, Ahmed et al. [100] and Habibi et al. [97] reported a higher value of 10% for the  
518 discount rate.

519 For the project baseline values, using a WACC of 0.08, it is expected that the investment will  
520 be recovered in 11.7 years, according to the discounted payback method (DPB). The net present  
521 value (NPV) over the project lifespan of 25 years is \$3,165,600, yielding an internal rate of return  
522 (IRR) of 0.128. Furthermore, a profitability index (PI) of 44% is obtained, i.e., an accumulated  
523 profit of up to 44% based on the initial investment.

### 524 3.5.2. Sensitivity analysis

525 A sensitivity analysis of the NPV for various values of the WACC ranging from 0 to 0.20 is  
526 illustrated in Fig. 9. As the IRR is equal to 0.128, the investment is profitable only for WACC  
527 values below 0.128. The project achieves a benefit higher than the initial investment, indicated by  
528 a PI grater than unity, when the WACC is below 0.05.

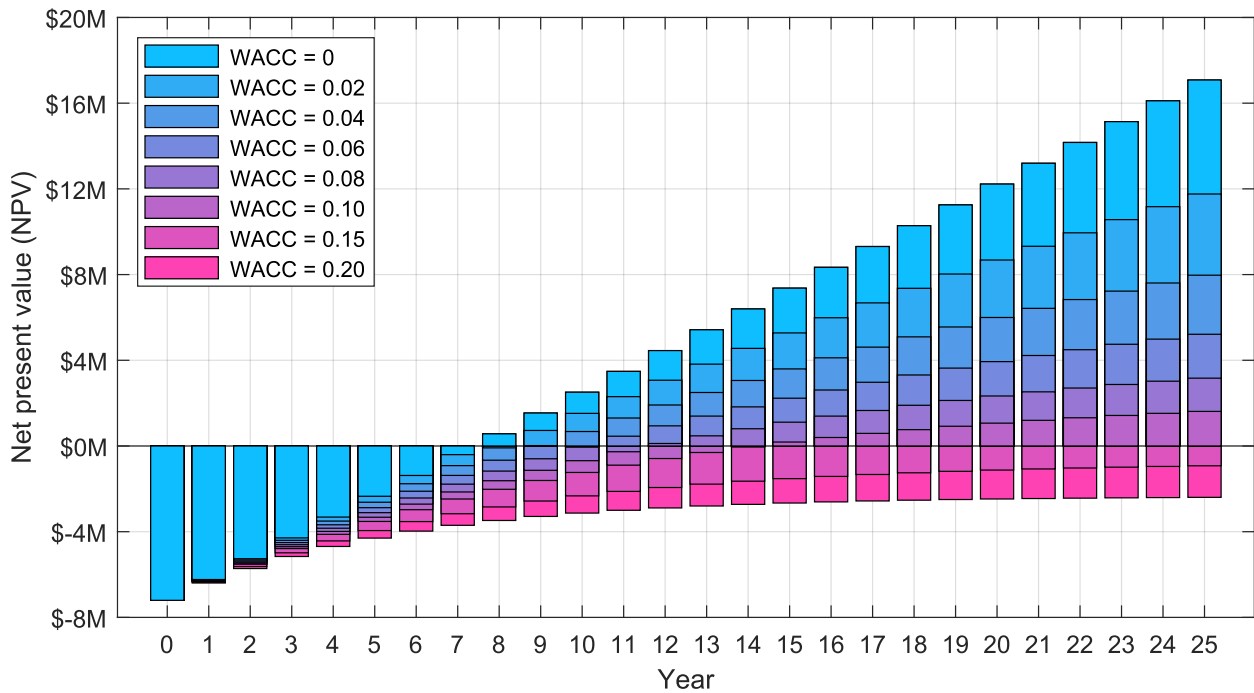


Figure 9: Sensitivity analysis for different values of the WACC.

529 Fig. 10 presents a sensitivity analysis of several key factors influencing the installation of an  
 530 ORC system onboard a shuttle tanker ship. The analysis examines the impacts of diesel price,  
 531 government subsidy percentage, CO<sub>2</sub> emissions price, and utilization factor on various economic  
 532 indicators.

533 Firstly, the effect of the utilization factor, measured in days, is evaluated. As the utilization  
 534 factor increases from 290 to 360 days, the discounted payback period decreases from around 17.5  
 535 years to approximately 11.5 years. The NPV shows can reach approximately \$3.2M with higher  
 536 utilization. Likewise, the PI rises from around 0.16 to 0.44, and the IRR improves slightly from  
 537 approximately 0.1 to 0.13. A high utilization factor leads to better economic outcomes, but is not  
 538 a particularly influential parameter within the range of values examined.

539 The second parameter considered is the price of CO<sub>2</sub> emissions. As the price of CO<sub>2</sub> emis-  
 540 sions rises from \$0 per tonne to \$175 per tonne, the discounted payback period decreases from  
 541 about 15.5 years to approximately 9.5 years. Correspondingly, the NPV increases from around  
 542 \$1.7M to \$4.6M, reflecting the advantageous economic impact of higher CO<sub>2</sub> prices. The PI also

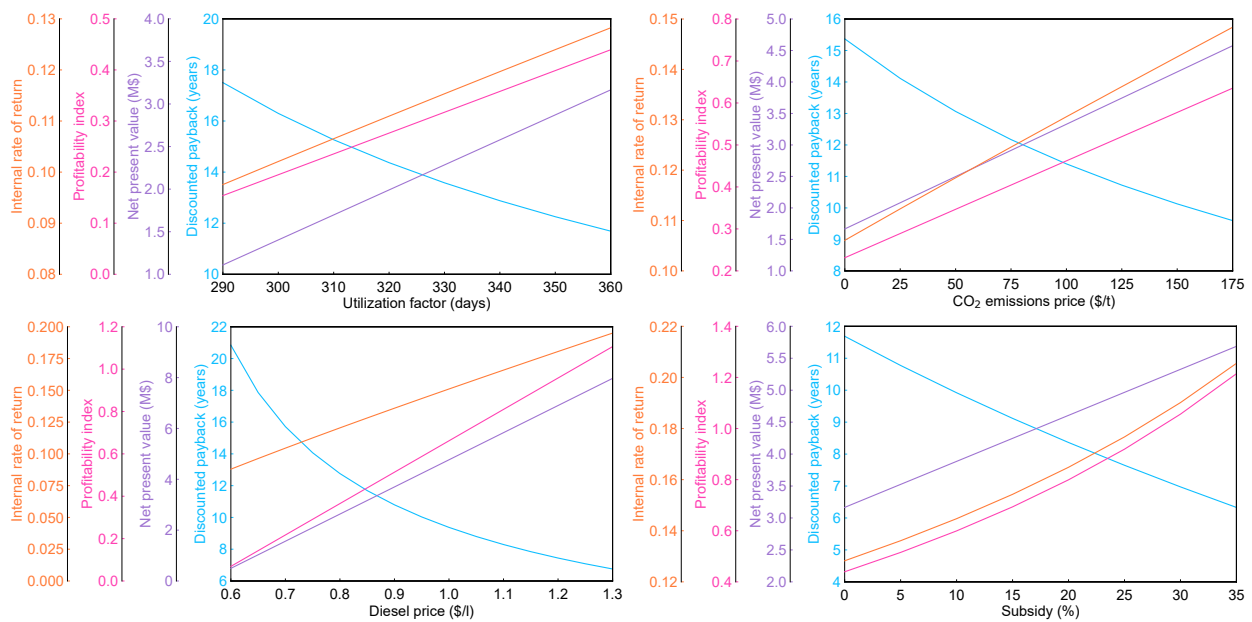


Figure 10: Sensitivity assessment of the different economic parameters as a function of the diesel price (*top*), biomass price (*center*) and percentage of subsidy (*bottom*).

543 increases from 0.23 to about 0.64 with the rise in CO<sub>2</sub> price. Similarly, the IRR improves from  
 544 approximately 0.1 to 0.15, indicating that higher CO<sub>2</sub> prices make the investment more financially  
 545 attractive.

546 The third parameter considered is the diesel price, which is a critical variable substantially  
 547 affecting the economic performance of the ORC system. As the diesel price increases from \$0.6  
 548 per liter to \$1.3 per liter, the discounted payback period decreases sharply from approximately  
 549 20.8 years to around 6.7 years. Concurrently, the NPV shows a notable increase from \$0.5M to  
 550 about \$8M. The PI also rises drastically from 0.07 to around 1.1 as the diesel price increases,  
 551 indicating an accumulated profit of up to 110% based on the initial investment. Additionally, the  
 552 IRR remarkably improves from 0.09 to approximately 0.2 with the rising diesel price, highlighting  
 553 enhanced project viability under higher diesel costs.

554 The last parameter analyzed is the percentage of non-refundable subsidies on the capital in-  
 555 vestment. Increasing the subsidy from 0% to 35% significantly reduces the discounted payback  
 556 period from approximately 11.7 years to around 6.3 years. Similarly, the NPV increases from

557 roughly \$3.2M to \$5.7M with higher subsidy rates. The PI exhibits a substantial increase from  
558 around 0.44 to 1.21 as the subsidy percentage rises. Furthermore, the IRR improves from 0.13 to  
559 0.21, demonstrating the beneficial impact of subsidies on the project's financial performance.

#### 560 **4. Conclusion**

561 This study has demonstrated the techno-economic viability of implementing a regenerative  
562 ORC cycle for waste heat recovery from marine diesel engines using acetone as the working fluid.  
563 The system is designed to generate an additional 2.2 MW<sub>e</sub> of electric power from the thermal  
564 energy contained in the exhaust gases of two diesel generators with 14.4 MW<sub>e</sub> each of nominal  
565 electric power installed on board a DC cargo distribution vessel. The key conclusions derived from  
566 this study are presented in the following points:

- 567 • Considering the overall energy performance of the system, it achieves a net overall electrical  
568 efficiency of 48.7%, meaning nearly half of the input energy is converted into electrical  
569 power to supply the loads and propulsion system. Additionally, 3.1 MW of waste heat  
570 (4.8% of the input energy) is recovered through engine jacket water heat exchangers for the  
571 production of HSW, enabling the CHP system to reach a net overall efficiency of 53.5%.  
572 At 85% generator load, the system demonstrates a net electrical efficiency of 8.45% and a  
573 thermodynamic efficiency of 18.73%.
- 574 • Implementing this technology in a DC distribution vessel results in a significant reduction  
575 in CO<sub>2</sub> emissions. It is estimated that adopting the ORC system could achieve an annual de-  
576 crease of 18.5% in CO<sub>2</sub> emissions and diesel consumption compared to a reference scenario  
577 without this technology.
- 578 • The financial analysis indicates that the ORC provides a cumulative return on investment of  
579 44%, with a payback period of 11.7 years and an internal rate of return of 12.8%, suggesting  
580 it could be a worthwhile investment, particularly when considering potential incentives for  
581 carbon reduction and subsidy.

- By reducing diesel consumption, the ORC system mitigates the financial impact of fuel price fluctuations, which is particularly relevant for maritime operations where fuel costs represent a significant portion of total operating expenses. The system offers a strategic advantage in an industry increasingly affected by rising fuel prices and stricter emissions regulations.

The comprehensive evaluation of the ORC unit presented in this study, including energy analysis, economic and environmental assessments, off-design optimization using real ship routes, as well as a detailed sensitivity analysis, fills a significant gap in the literature. By integrating technical performance, economic viability, and environmental impact, this approach provides a holistic and practical perspective that is essential for real-world applications. The inclusion of off-design optimization with real ship routes ensures that the system's performance is accurately assessed under varying operational conditions, making this research particularly valuable for the maritime sector. These insights are key in guiding the adoption of ORC technology in actual marine operations, offering a pathway to more efficient, cost-effective, and environmentally sustainable solutions in the industry.

## Nomenclature

### Symbols

$\dot{m}$  Mass flow rate [ $\text{kg}\cdot\text{s}^{-1}$ ]

$\dot{Q}$  Heat flow rate [kW]

$\dot{W}$  Power [kW]

$\eta$  Efficiency

$c_p$  Mass heat capacity at constant pressure [ $\text{kJ}\cdot\text{kg}^{-1}\cdot\text{K}^{-1}$ ]

$H$  Enthalpy [kJ]

$h$  Mass enthalpy [ $\text{kJ}\cdot\text{kg}^{-1}$ ]

$n$  Life span

$P$  Power [kW]

$p$  Pressure [bar]

$S$  Entropy [ $\text{kJ}\cdot\text{K}^{-1}$ ]

$s$  Mass entropy [ $\text{kJ}\cdot\text{kg}^{-1}\text{K}^{-1}$ ]

$T$  Temperature [ $^{\circ}\text{C}$ ]

$t$  Time period

$U$  Global heat transfer coefficient [ $\text{W}\cdot\text{m}^{-2}\cdot\text{K}^{-1}$ ]

$V$  Voltage [V]

### Subscripts

$a$  Ambient

$bottom$  Bottoming power cycle

$cond$  Condenser

620	<i>conv</i>	Power conversion	646	AC	Alternating current
621	<i>e</i>	Electrical	647	CEPCI	Chemical Engineering Plant Cost Index
622	<i>eg</i>	Exhaust gas	648		
623	<i>em</i>	Electromechanical	649	CHP	Combined heat and power
624	<i>evap</i>	Evaporator	650	DC	Direct current
625	<i>exp</i>	Expander	651	DFCI	Direct fixed-capital investment
626	<i>f</i>	Feedstock or fuel	652	DG	Diesel generator
627	<i>gen</i>	Generator	653	DPB	Discounted payback
628	<i>gross</i>	Gross electricity	654	EG	Exhaust gas
629	<i>htf</i>	Heat transfer fluid	655	FCI	Fixed-capital investment
630	<i>hx</i>	Heat exchanger	656	GWP	Global warming potential
631	<i>i</i>	Isentropic	657	HRSG	Heat recovery steam generator
632	<i>ip</i>	inner pipe	658	HSW	Hot sanitary water
633	<i>k</i>	Component	659	HT	High temperature
634	<i>l</i>	loss	660	HTF	Heat transfer fluid
635	<i>lm</i>	logarithmic mean	661	HTHX	High-temperature heat exchanger
636	<i>m</i>	Mechanical	662	HTS	High-temperature source
637	<i>net</i>	Net electricity	663	HX	Heat exchanger
638	<i>og</i>	Off-gas	664	IFCI	Indirect fixed-capital investment
639	<i>op</i>	outer pipe	665	INV	Investment
640	<i>pump</i>	Pump	666	IRR	Internal rate of return
641	<i>reg</i>	Regenerator	667	LT	Low temperature
642	<i>sw</i>	Sea water	668	NCF	Net cash flow
643	<i>wf</i>	Working fluid	669	NPFA	National Fire Protection Association
644	<b>Abbreviations</b>		670	NPV	Net present value
645	<i>TIT</i>	Turbine inlet temperature	671	O&M	Operational and maintenance
			672	ODP	Ozone depletion potential

673	ORC	Organic Rankine cycle	677	WACC	Weighted average cost of capital
674	PEC	Purchase equipment cost	678	WF	Working fluid
675	PI	Profitability index	679	WHR	Waste-heat recovery
676	SFOC	Specific fuel oil consumption			

## 680 **CRedit authorship contribution statement**

681 **D. Sánchez-Lozano:** Conceptualization, Data curation, Formal analysis, Investigation, Method-  
682 ology, Software, Validation, Visualization, Writing - Original Draft, Writing - Review & Editing.  
683 **R. Aguado:** Conceptualization, Formal analysis, Investigation, Methodology, Validation, Visual-  
684 ization, Writing - Original Draft, Writing - Review & Editing. **A. Escámez:** Conceptualization,  
685 Formal analysis, Investigation, Methodology, Software, Visualization, Writing - Review & Edit-  
686 ing. **J.A. Hernández-Torres:** Conceptualization, Investigation, Methodology, Resources, Visu-  
687 alization. **J.P. Torreglosa:** Conceptualization, Funding acquisition, Investigation, Methodology,  
688 Project administration, Resources, Supervision, Validation. **D. Vera:** Conceptualization, Funding  
689 acquisition, Investigation, Methodology, Project administration, Supervision, Validation.

## 690 **Funding**

691 This work was supported in part by “Programa Operativo FEDER 2014-2020” and “Consejería  
692 de Economía, Conocimiento, Empresas y Universidad de la Junta de Andalucía” under Project  
693 UHU-202051 and in part by CEI·MAR through the scientific improvement axis of the CEI·MAR  
694 2023 Plan: Research Projects of early-career Ph.D. CEI·MAR 2023 under Project CEI-JD-12.

695 Roque Aguado, Antonio Escámez and Daniel Sánchez acknowledge financial support from  
696 Ministerio de Ciencia, Innovación y Universidades under the FPU Program (Refs. FPU19/00930,  
697 FPU22/00741, FPU22/00879, respectively).

698 **References**

- 699 [1] M. Soffiato, C. A. Frangopoulos, G. Manente, S. Rech, A. Lazzaretto, Design optimization of ORC systems  
700 for waste heat recovery on board a LNG carrier, *Energy Convers. Manag.* 92 (2015) 523–534. doi:10.1016/  
701 j.enconman.2014.12.085.
- 702 [2] IRENA, A pathway to decarbonise the shipping sector by 2050, Tech. rep., IRENA (2021).
- 703 [3] IMO, Fourth imo ghg study, Tech. rep., IMO (International Maritime Organization) (2020).
- 704 [4] S. B. Roslan, D. Konovessis, Z. Y. Tay, Sustainable hybrid marine power systems for power management  
705 optimisation: A review, *Energies* 15 (24) (2022). doi:10.3390/en15249622.
- 706 [5] B. Zahedi, L. E. Norum, K. B. Ludvigsen, Optimized efficiency of all-electric ships by DC hybrid power  
707 systems, *J. Power Sources* 255 (2014) 341–354. doi:10.1016/j.jpowsour.2014.01.031.
- 708 [6] D. Micheli, S. Clemente, R. Taccani, Chapter 2 - energy systems on board ships, in: F. Baldi, A. Coraddu, M. E.  
709 Mondejar (Eds.), *Sustainable Energy Systems on Ships*, Elsevier, 2022, pp. 27–78. doi:10.1016/B978-0-  
710 12-824471-5.00008-6.
- 711 [7] A. Haseltalab, M. A. Botto, R. R. Negenborn, Model predictive dc voltage control for all-electric ships, *Control*  
712 *Engineering Practice* 90 (2019) 133–147. doi:10.1016/j.conengprac.2019.06.018.
- 713 [8] A. Haseltalab, F. Wani, R. R. Negenborn, Multi-level model predictive control for all-electric ships with hybrid  
714 power generation, *Int. J. Elec. Power Energy Syst.* 135 (2022) 107484. doi:10.1016/j.ijepes.2021.  
715 107484.
- 716 [9] C. Nuchturee, T. Li, H. Xia, Energy efficiency of integrated electric propulsion for ships – A review, *Renew,*  
717 *Sust, Energ, Rev*, 134 (2020) 110145. doi:10.1016/j.rser.2020.110145.
- 718 [10] R. Geertsma, R. Negenborn, K. Visser, J. Hopman, Design and control of hybrid power and propulsion systems  
719 for smart ships: A review of developments, *Appl. Energy* 194 (2017) 30–54. doi:10.1016/j.apenergy.  
720 2017.02.060.
- 721 [11] D. V. Singh, E. Pedersen, A review of waste heat recovery technologies for maritime applications, *Energy*  
722 *Convers. Manag.* 111 (2016) 315–328. doi:10.1016/j.enconman.2015.12.073.
- 723 [12] C. Sellers, Field operation of a 125kW ORC with ship engine jacket water, *Energy Procedia* 129 (2017)  
724 495–502, 4th International Seminar on ORC Power Systems September 13-15th 2017 POLITECNICO DI MI-  
725 LANOBOVISA CAMPUSMILANO, ITALY. doi:10.1016/j.egypro.2017.09.168.
- 726 [13] R. Pili, A. Romagnoli, K. Kamossa, A. Schuster, H. Spliethoff, C. Wieland, Organic Rankine Cycles (ORC)  
727 for mobile applications – Economic feasibility in different transportation sectors, *Appl. Energy* 204 (2017)  
728 1188–1197. doi:10.1016/j.apenergy.2017.04.056.

- 729 [14] M. E. Mondejar, F. Ahlgren, M. Thern, M. Genrup, Quasi-steady state simulation of an organic Rankine cy-  
730 cle for waste heat recovery in a passenger vessel, *Appl. Energy* 185 (2017) 1324–1335, clean, Efficient and  
731 Affordable Energy for a Sustainable Future. [doi:10.1016/j.apenergy.2016.03.024](https://doi.org/10.1016/j.apenergy.2016.03.024).
- 732 [15] M. Casisi, P. Pinamonti, M. Reini, Increasing the energy efficiency of an internal combustion engine for ship  
733 propulsion with bottom ORCs, *Applied Sciences* 10 (19) (2020).
- 734 [16] Z. Mat Nawi, S. Kamarudin, S. Sheikh Abdullah, S. Lam, The potential of exhaust waste heat recovery (WHR)  
735 from marine diesel engines via organic rankine cycle, *Energy* 166 (2019) 17–31. [doi:10.1016/j.energy.](https://doi.org/10.1016/j.energy.2018.10.064)  
736 [2018.10.064](https://doi.org/10.1016/j.energy.2018.10.064).
- 737 [17] J. Song, Y. Song, C. wei Gu, Thermodynamic analysis and performance optimization of an Organic Rankine  
738 Cycle (ORC) waste heat recovery system for marine diesel engines, *Energy* 82 (2015) 976–985. [doi:10.](https://doi.org/10.1016/j.energy.2015.01.108)  
739 [1016/j.energy.2015.01.108](https://doi.org/10.1016/j.energy.2015.01.108).
- 740 [18] F. Catapano, A. Frazzica, A. Freni, M. Manzan, D. Micheli, V. Palomba, P. Sementa, B. Vaglieco, Development  
741 and experimental testing of an integrated prototype based on Stirling, ORC and a latent thermal energy storage  
742 system for waste heat recovery in naval application, *Appl. Energy* 311 (2022) 118673. [doi:10.1016/j.](https://doi.org/10.1016/j.apenergy.2022.118673)  
743 [apenergy.2022.118673](https://doi.org/10.1016/j.apenergy.2022.118673).
- 744 [19] O. Konur, O. Yuksel, S. Aykut Korkmaz, C. Ozgur Colpan, O. Y. Saatcioglu, B. Koseoglu, Operation-dependent  
745 exergetic sustainability assessment and environmental analysis on a large tanker ship utilizing Organic Rankine  
746 cycle system, *Energy* 262 (2023) 125477. [doi:10.1016/j.energy.2022.125477](https://doi.org/10.1016/j.energy.2022.125477).
- 747 [20] M.-H. Yang, R.-H. Yeh, Thermodynamic and economic performances optimization of an organic Rankine  
748 cycle system utilizing exhaust gas of a large marine diesel engine, *Appl. Energy* 149 (2015) 1–12. [doi:](https://doi.org/10.1016/j.apenergy.2015.03.083)  
749 [10.1016/j.apenergy.2015.03.083](https://doi.org/10.1016/j.apenergy.2015.03.083).
- 750 [21] P. Pallis, E. Varvagiannis, K. Braimakis, T. Roumpedakis, A. D. Leontaritis, S. Karellas, Development, exper-  
751 imental testing and techno-economic assessment of a fully automated marine organic rankine cycle prototype  
752 for jacket cooling water heat recovery, *Energy* 228 (2021) 120596. [doi:10.1016/j.energy.2021.120596](https://doi.org/10.1016/j.energy.2021.120596).
- 753 [22] J. Zeng, W. Chen, W. Yu, L. Lyu, W. Luo, S. Xue, Application analysis of organic Rankine cycle technology  
754 to recover ship waste heat and construction of experimental bench, in: *2022 7th International Conference on*  
755 *Power and Renewable Energy (ICPRE), 2022*, pp. 1063–1068. [doi:10.1109/ICPRE55555.2022.9960614](https://doi.org/10.1109/ICPRE55555.2022.9960614).
- 756 [23] C. Ng, I. C. K. Tam, D. Wu, Thermo-economic performance of an organic Rankine cycle system recovering  
757 waste heat onboard an offshore service vessel, *J. Mar. Sci. Eng.* 8 (5) (2020). [doi:10.3390/jmse8050351](https://doi.org/10.3390/jmse8050351).
- 758 [24] N. Doerry, J. Amy, Mvdc shipboard power system considerations for electromagnetic railguns, 2015.
- 759 [25] J. P. Torreglosa, D. López-García, J. Hernández-Torres, D. Vera, A. P. Vallés, J. Clavijo-Camacho, Mvdc elec-

- 760 tric propulsion systems for integrating waste heat recovery systems in marine transport, *IEEE Trans. Transp.*  
761 *Electrif.* (2024) 1–1 [doi:10.1109/TTE.2024.3356655](https://doi.org/10.1109/TTE.2024.3356655).
- 762 [26] Wärtsilä, Wärtsilä 46f product guide, Tech. rep., Wärtsilä (2020).
- 763 [27] R. Aguado, A. Baccioli, A. Liponi, D. Vera, Continuous decentralized hydrogen production through alkaline  
764 water electrolysis powered by an oxygen-enriched air integrated biomass gasification combined cycle, *Energy*  
765 *Convers. Manag.* 289 (2023) 117149. [doi:10.1016/j.enconman.2023.117149](https://doi.org/10.1016/j.enconman.2023.117149).
- 766 [28] D. Vera, F. Jurado, J. Carpio, S. Kamel, Biomass gasification coupled to an EFGT-ORC combined system to  
767 maximize the electrical energy generation: A case applied to the olive oil industry, *Energy* 144 (2018) 41–53.  
768 [doi:10.1016/j.energy.2017.11.152](https://doi.org/10.1016/j.energy.2017.11.152).
- 769 [29] A. Mana, S. Kaitouni, T. Kousksou, A. Jamil, Enhancing sustainable energy conversion: Comparative study of  
770 superheated and recuperative ORC systems for waste heat recovery and geothermal applications, with focus on  
771 4E performance, *Energy* 284 (2023) 128654. [doi:10.1016/j.energy.2023.128654](https://doi.org/10.1016/j.energy.2023.128654).
- 772 [30] B. de Mena, D. Vera, F. Jurado, M. Ortega, Updraft gasifier and ORC system for high ash content biomass: A  
773 modelling and simulation study, *Fuel Process. Technol.* 156 (2017) 394–406. [doi:https://doi.org/10.](https://doi.org/10.1016/j.fuproc.2016.09.031)  
774 [1016/j.fuproc.2016.09.031](https://doi.org/10.1016/j.fuproc.2016.09.031).
- 775 [31] M. Bahrami, F. Pourfayaz, A. Kasaeian, Low global warming potential (GWP) working fluids (WFs) for  
776 Organic Rankine Cycle (ORC) applications, *Energy Reports* 8 (2022) 2976–2988. [doi:10.1016/j.egypr.](https://doi.org/10.1016/j.egypr.2022.01.222)  
777 [2022.01.222](https://doi.org/10.1016/j.egypr.2022.01.222).
- 778 [32] S. Douvartzides, I. Karmalis, Working fluid selection for the Organic Rankine Cycle (ORC) exhaust heat recov-  
779 ery of an internal combustion engine power plant, *IOP Conference Series: Materials Science and Engineering*  
780 161 (1) (2016) 012087. [doi:10.1088/1757-899X/161/1/012087](https://doi.org/10.1088/1757-899X/161/1/012087).
- 781 [33] Z. Ge, J. Li, Y. Duan, Z. Yang, Z. Xie, Thermodynamic performance analyses and optimization of dual-loop  
782 organic Rankine cycles for internal combustion engine waste heat recovery, *Appl. Sci.* 9 (4) (2019).
- 783 [34] National Fire Protection Association, NFPA 704 Standard System for the Identification of the Hazards of  
784 Materials for Emergency Response.
- 785 [35] D. Luo, A. Mahmoud, F. Cogswell, Evaluation of Low-GWP fluids for power generation with Organic Rankine  
786 Cycle, *Energy* 85 (2015) 481–488. [doi:10.1016/j.energy.2015.03.109](https://doi.org/10.1016/j.energy.2015.03.109).
- 787 [36] U. Drescher, D. Brüggemann, Fluid selection for the Organic Rankine Cycle (ORC) in biomass power and heat  
788 plants, *Appl. Therm. Eng.* 27 (1) (2007) 223–228. [doi:https://doi.org/10.1016/j.applthermaleng.](https://doi.org/10.1016/j.applthermaleng.2006.04.024)  
789 [2006.04.024](https://doi.org/10.1016/j.applthermaleng.2006.04.024).
- 790 [37] J. Bao, L. Zhao, A review of working fluid and expander selections for organic Rankine cycle, *Renew. Sust.*

- 791 Energ. Rev. 24 (2013) 325–342. doi:10.1016/j.rser.2013.03.040.
- 792 [38] Thermoflow inc, Available online: <https://www.thermoflow.com/index.html>, (accessed on 05 Jan.  
793 2024).
- 794 [39] A. Pantaleo, M. Simpson, G. Rotolo, E. Distaso, O. Oyewunmi, P. Sapin, P. de Palma, C. Markides, Ther-  
795 moeconomic optimisation of small-scale organic Rankine cycle systems based on screw vs. piston expander  
796 maps in waste heat recovery applications, Energy Convers. Manag. 200 (2019) 112053. doi:10.1016/j.  
797 enconman.2019.112053.
- 798 [40] Özkan Köse, Y. Koç, H. Yağlı, Performance improvement of the bottoming steam Rankine cycle (SRC) and  
799 organic Rankine cycle (ORC) systems for a triple combined system using gas turbine (GT) as topping cycle,  
800 Energy Convers. Manag. 211 (2020) 112745. doi:10.1016/j.enconman.2020.112745.
- 801 [41] U. E. P. Agency, Transitioning to low-gwp alternatives, Tech. rep., U.S. Environmental Protection Agency  
802 (2016).
- 803 [42] X. Dai, L. Shi, W. Qian, Review of the working fluid thermal stability for organic rankine cycles, Journal of  
804 Thermal Science 28 (4) (2019) 597–607. doi:10.1007/s11630-019-1119-3.  
805 URL <https://doi.org/10.1007/s11630-019-1119-3>
- 806 [43] I. Meziane, Y. Fenard, N. Delort, O. Herbinet, J. Bourgalais, A. Ramalingam, K. A. Heufer, F. Battin-Leclerc,  
807 Experimental and modeling study of acetone combustion, Combustion and Flame 257 (2023) 112416, james  
808 A. Miller Special Commemorative Issue. doi:10.1016/j.combustflame.2022.112416.
- 809 [44] J. G. DAVOUD, C. N. HINSHELWOOD, Thermal decomposition of acetone, Nature 144 (3656) (1939) 909–  
810 910. doi:10.1038/144909a0.
- 811 [45] S. Lebedevas, T. Čepaitis, Complex use of the main marine diesel engine high- and low-temperature waste heat  
812 in the organic Rankine cycle, J. Mar. Sci. Eng. 12 (3) (2024). doi:10.3390/jmse12030521.
- 813 [46] D. Sánchez-Lozano, A. Escámez, R. Aguado, S. Oulbi, R. Hadria, D. Vera, Techno-economic assessment of an  
814 off-grid biomass gasification CHP plant for an olive oil mill in the region of Marrakech-Safi, Morocco, Appl.  
815 Sci. 13 (10) (2023). doi:10.3390/app13105965.
- 816 [47] M. Bianchi, L. Branchini, A. De Pascale, F. Melino, V. Orlandini, A. Peretto, D. Archetti, F. Campana, T. Fer-  
817 rari, N. Rossetti, Techno-economic analysis of ORC in gas compression stations taking into account actual  
818 operating conditions, Energy Procedia 129 (2017) 543–550. doi:10.1016/j.egypro.2017.09.182.
- 819 [48] M. M. L. Reis, W. L. Gallo, Study of waste heat recovery potential and optimization of the power production  
820 by an organic Rankine cycle in an FPSO unit, Energy Convers. Manag. 157 (2018) 409–422. doi:10.1016/  
821 j.enconman.2017.12.015.

- 822 [49] J.-S. Kim, D.-Y. Kim, Energy, exergy, and economic (3E) analysis of SOFC-GT-ORC hybrid systems for  
823 ammonia-fueled ships, *J. Mar. Sci. Eng.* 11 (11) (2023).
- 824 [50] W. Chen, B. Fu, J. Zeng, W. Luo, Research on the operational performance of organic Rankine cycle system for  
825 waste heat recovery from large ship main engine, *Appl. Sci.* 13 (14) (2023). doi:10.3390/app13148543.
- 826 [51] G. Kosmadakis, P. Neofytou, Reversible high-temperature heat pump/ORC for waste heat recovery in various  
827 ships: A techno-economic assessment, *Energy* 256 (2022) 124634. doi:10.1016/j.energy.2022.124634.
- 828 [52] S. Lion, R. Taccani, I. Vlaskos, P. Scrocco, X. Vouvakos, L. Kaiktsis, Thermodynamic analysis of waste heat  
829 recovery using Organic Rankine Cycle (ORC) for a two-stroke low speed marine Diesel engine in IMO Tier II  
830 and Tier III operation, *Energy* 183 (2019) 48–60. doi:10.1016/j.energy.2019.06.123.
- 831 [53] M. Astolfi, M. C. Romano, P. Bombarda, E. Macchi, Binary ORC (Organic Rankine Cycles) power plants  
832 for the exploitation of medium–low temperature geothermal sources – Part B: Techno-economic optimization,  
833 *Energy* 66 (2014) 435–446. doi:10.1016/j.energy.2013.11.057.
- 834 [54] S. M. Camporeale, A. M. Pantaleo, P. D. Ciliberti, B. Fortunato, Cycle configuration analysis and techno-  
835 economic sensitivity of biomass externally fired gas turbine with bottoming ORC, *Energy Convers. Manag.*  
836 105 (2015) 1239–1250. doi:10.1016/j.enconman.2015.08.069.
- 837 [55] P. Das, D. Mondal, M. Ashrafur Islam, M. Afroj Lily, Thermodynamic performance evaluation of a solar pow-  
838 ered Organic Rankine cycle (ORC) and dual cascading vapor compression cycle (DCVCC): Power generation  
839 and cooling effect, *Energy Convers. Manag.* X 23 (2024) 100662. doi:10.1016/j.ecmx.2024.100662.
- 840 [56] X. Zhou, Z. Xin, W. Tang, K. Sheng, Z. Wu, Comparative study for waste heat recovery in immersion cooling  
841 data centers with district heating and organic Rankine cycle (ORC), *Appl. Therm. Eng.* 242 (2024) 122479.  
842 doi:10.1016/j.applthermaleng.2024.122479.
- 843 [57] V. Zare, A comparative exergoeconomic analysis of different ORC configurations for binary geothermal power  
844 plants, *Energy Convers. Manag.* 105 (2015) 127–138. doi:10.1016/j.enconman.2015.07.073.
- 845 [58] K. Braimakis, A. Charalampidis, S. Karellas, Techno-economic assessment of a small-scale biomass ORC-  
846 CHP for district heating, *Energy Convers. Manag.* 247 (2021) 114705. doi:10.1016/j.enconman.2021.  
847 114705.
- 848 [59] Y. Jang, J. Lee, Optimizations of the organic Rankine cycle-based domestic CHP using biomass fuel, *Energy*  
849 *Convers. Manag.* 160 (2018) 31–47. doi:10.1016/j.enconman.2018.01.025.
- 850 [60] S. Zhang, L. Li, E. Huo, Y. Yu, R. Huang, S. Wang, Parameters analysis and techno-economic comparison of  
851 various ORCs and sCO<sub>2</sub> cycles as the power cycle of Lead–Bismuth molten nuclear micro-reactor, *Energy* 295  
852 (2024) 131103. doi:10.1016/j.energy.2024.131103.

- 853 [61] E. Akrami, A. Chitsaz, H. Nami, S. Mahmoudi, Energetic and exergoeconomic assessment of a multi-  
854 generation energy system based on indirect use of geothermal energy, *Energy* 124 (2017) 625–639. doi:  
855 [10.1016/j.energy.2017.02.006](https://doi.org/10.1016/j.energy.2017.02.006).
- 856 [62] E. Gholamian, A. Habibollahzade, V. Zare, Development and multi-objective optimization of geothermal-based  
857 organic Rankine cycle integrated with thermoelectric generator and proton exchange membrane electrolyzer for  
858 power and hydrogen production, *Energy Convers. Manag.* 174 (2018) 112–125. doi:[10.1016/j.enconman.](https://doi.org/10.1016/j.enconman.2018.08.027)  
859 [2018.08.027](https://doi.org/10.1016/j.enconman.2018.08.027).
- 860 [63] A. Behzadi, E. Gholamian, E. Houshfar, A. Habibollahzade, Multi-objective optimization and exergoeconomic  
861 analysis of waste heat recovery from Tehran’s waste-to-energy plant integrated with an ORC unit, *Energy* 160  
862 (2018) 1055–1068. doi:[10.1016/j.energy.2018.07.074](https://doi.org/10.1016/j.energy.2018.07.074).
- 863 [64] S. Mahmoudi, A. Ghavimi, Thermo-economic analysis and multi objective optimization of a molten carbonate  
864 fuel cell – Supercritical carbon dioxide – Organic Rankine cycle integrated power system using liquefied natural  
865 gas as heat sink, *Appl. Therm. Eng.* 107 (2016) 1219–1232. doi:[10.1016/j.applthermaleng.2016.07.](https://doi.org/10.1016/j.applthermaleng.2016.07.003)  
866 [003](https://doi.org/10.1016/j.applthermaleng.2016.07.003).
- 867 [65] D. Roy, S. Samanta, S. Roy, A. Smallbone, A. Paul Roskilly, Fuel cell integrated carbon negative power  
868 generation from biomass, *Appl. Energy* 331 (2023) 120449. doi:[10.1016/j.apenergy.2022.120449](https://doi.org/10.1016/j.apenergy.2022.120449).
- 869 [66] S. Baral, J. Šebo, Techno-economic assessment of green hydrogen production integrated with hybrid and or-  
870 ganic rankine cycle (orc) systems, *Heliyon* 10 (4) (2024) e25742. doi:[10.1016/j.heliyon.2024.e25742](https://doi.org/10.1016/j.heliyon.2024.e25742).
- 871 [67] F. Tanbar, R. Febriyanto, H. M. Ariyadi, A. D. Nugraha, A. A. Simaremare, E. Supriyanto, M. Triani, M. A.  
872 Muflikhun, Techno-economic studies of low gwp-organic rankine cycle for low-level geothermal waste heat  
873 utilization in remote island of indonesia, *Case Studies in Thermal Engineering* 65 (2025) 105385. doi:[10.](https://doi.org/10.1016/j.csite.2024.105385)  
874 [1016/j.csite.2024.105385](https://doi.org/10.1016/j.csite.2024.105385).
- 875 [68] t. E. Australian Government Department of Climate Change, Energy, Water, Acetone, Available online:  
876 <https://www.dcceew.gov.au/environment/protection/npi/substances/fact-sheets/acetone>, (accessed on 25 Feb.  
877 2025).
- 878 [69] NOAA (National Oceanic and Atmospheric Administration), Acetone cameo chemicals, Available online:  
879 <https://cameochemicals.noaa.gov/chris/CYP.pdf>, (accessed on 25 Feb. 2025).
- 880 [70] International Labour Organization (ILO), Cyclopentane - international chemical safety card (icsc 0353),  
881 Available online: [https://chemicalsafety.ilo.org/dyn/icsc/showcard.display?p\\_lang=en&p\\_](https://chemicalsafety.ilo.org/dyn/icsc/showcard.display?p_lang=en&p_version=2&p_card_id=0353)  
882 [version=2&p\\_card\\_id=0353](https://chemicalsafety.ilo.org/dyn/icsc/showcard.display?p_lang=en&p_version=2&p_card_id=0353), accessed: 2025-02-25.
- 883 [71] NOAA (National Oceanic and Atmospheric Administration), Acetone cameo chemicals, Available online:

- 884 <https://cameochemicals.noaa.gov/chris/ACT.pdf>, (accessed on 25 Feb. 2025).
- 885 [72] G. V. Ochoa, C. A. Peñaloza, J. P. Rojas, [Thermoeconomic Modelling and Parametric Study of a Simple ORC](#)  
886 [for the Recovery of Waste Heat in a 2 MW Gas Engine under Different Working Fluids](#), *Applied Sciences*  
887 9 (21) (2019). doi:10.3390/app9214526.  
888 URL <https://www.mdpi.com/2076-3417/9/21/4526>
- 889 [73] G. V. Ochoa, C. Isaza-Roldan, J. Duarte Forero, Economic and exergo-advance analysis of a waste heat recov-  
890 ery system based on regenerative organic rankine cycle under organic fluids with low global warming potential,  
891 *Energies* 13 (6) (2020). doi:10.3390/en13061317.
- 892 [74] P. Klonowicz, Łukasz Witanowski, Łukasz Jędrzejewski, T. Suchocki, P. Lampart, A turbine based do-  
893 mestic micro orc system, *Energy Procedia* 129 (2017) 923–930, 4th International Seminar on ORC Power  
894 Systems September 13-15th 2017POLITECNICO DI MILANO BOVISA CAMPUS MILANO, ITALY. doi:  
895 [10.1016/j.egypro.2017.09.112](https://doi.org/10.1016/j.egypro.2017.09.112).
- 896 [75] F. Ferrara, A. Gimelli, A. Luongo, Small-scale concentrated solar power (csp) plant: Orcs comparison for  
897 different organic fluids, *Energy Procedia* 45 (2014) 217–226, aTI 2013 - 68th Conference of the Italian Thermal  
898 Machines Engineering Association. doi:10.1016/j.egypro.2014.01.024.
- 899 [76] G. Valencia Ochoa, J. Cárdenas Gutierrez, J. Duarte Forero, Exergy, economic, and life-cycle assessment  
900 of orc system for waste heat recovery in a natural gas internal combustion engine, *Resources* 9 (1) (2020).  
901 doi:10.3390/resources9010002.
- 902 [77] E. Kocaman, C. Karakuş, H. Yağlı, Y. Koç, R. Yumrutaş, A. Koç, Pinch point determination and multi-objective  
903 optimization for working parameters of an orc by using numerical analyses optimization method, *Energy Con-*  
904 *version and Management* 271 (2022) 116301. doi:10.1016/j.enconman.2022.116301.
- 905 [78] I. Herrera-Orozco, G. Valencia-Ochoa, J. Duarte-Forero, Exergo-environmental assessment and multi-objective  
906 optimization of waste heat recovery systems based on Organic Rankine cycle configurations, *J. Clean. Prod.*  
907 288 (2021) 125679. doi:10.1016/j.jclepro.2020.125679.
- 908 [79] N. K. Choudhary, S. Karmakar, Thermoeconomic analysis of organic Rankine cycle with different working  
909 fluids for waste heat recovery from a coal-based thermal power plant, *J. Therm. Anal. Calorim.* (May 2024).  
910 doi:10.1007/s10973-024-13142-3.
- 911 [80] S. Schuster, C. N. Markides, A. J. White, Design and off-design optimisation of an organic Rankine cycle  
912 (ORC) system with an integrated radial turbine model, *Appl. Therm. Eng.* 174 (2020) 115192. doi:10.1016/  
913 [j.applthermaleng.2020.115192](https://doi.org/10.1016/j.applthermaleng.2020.115192).
- 914 [81] M. A. Chatzopoulou, S. Lecompte, M. D. Paepe, C. N. Markides, Off-design optimisation of organic Rankine

- 915 cycle (ORC) engines with different heat exchangers and volumetric expanders in waste heat recovery applica-  
916 tions, *Appl. Energy* 253 (2019) 113442. doi:10.1016/j.apenergy.2019.113442.
- 917 [82] F. Fatigati, D. Vittorini, Y. Wang, J. Song, C. N. Markides, R. Cipollone, Design and operational control strat-  
918 egy for optimum off-design performance of an orc plant for low-grade waste heat recovery, *Energies* 13 (21)  
919 (2020). doi:10.3390/en13215846.
- 920 [83] F. Baldi, F. Ahlgren, T.-V. Nguyen, M. Thern, K. Andersson, Energy and exergy analysis of a cruise ship,  
921 *Energies* 11 (10) (2018). doi:10.3390/en11102508.
- 922 [84] D. Tutunea, I. Dumitru, L. Racila, O. Otat, L. Matei, I. Geonea, Characterization of sunflower oil biodiesel as  
923 alternative for diesel fuel, in: N. Burnete, B. O. Varga (Eds.), *Proceedings of the 4th International Congress of*  
924 *Automotive and Transport Engineering (AMMA 2018)*, Springer International Publishing, 2019, pp. 172–180.  
925 doi:10.1007/978-3-319-94409-8\_21.
- 926 [85] E. A. Bouman, E. Lindstad, A. I. Riialand, A. H. Strømman, State-of-the-art technologies, measures, and  
927 potential for reducing GHG emissions from shipping – A review, *Transportation Research Part D: Transport*  
928 *and Environment* 52 (2017) 408–421. doi:10.1016/j.trd.2017.03.022.
- 929 [86] E. Baldasso, T. J. A. Gilormini, M. E. Mondejar, J. G. Andreasen, L. K. Larsen, J. Fan, F. Haglind, Or-  
930 ganic Rankine cycle-based waste heat recovery system combined with thermal energy storage for emission-  
931 free power generation on ships during harbor stays, *J. Clean. Prod.* 271 (2020) 122394. doi:10.1016/j.  
932 jclepro.2020.122394.
- 933 [87] S. Quoilin, M. V. D. Broek, S. Declaye, P. Dewallef, V. Lemort, Techno-economic survey of Organic Rankine  
934 Cycle (ORC) systems, *Renew. Sust. Energ. Rev.* 22 (2013) 168–186. doi:10.1016/j.rser.2013.01.028.
- 935 [88] I. Girgin, C. Ezgi, Design and thermodynamic and thermoeconomic analysis of an organic Rankine cycle for  
936 naval surface ship applications, *Energy Convers. Manag.* 148 (2017) 623–634. doi:10.1016/j.enconman.  
937 2017.06.033.
- 938 [89] S. Lemmens, Cost engineering techniques and their applicability for cost estimation of organic Rankine cycle  
939 systems, *Energies* 9 (7) (2016). doi:10.3390/en9070485.
- 940 [90] E. J. Cavalcanti, H. P. Motta, Exergoeconomic analysis of a solar-powered/fuel assisted Rankine cycle for  
941 power generation, *Energy* 88 (2015) 555–562. doi:10.1016/j.energy.2015.05.081.
- 942 [91] M. R. Goma, R. J. Mustafa, M. Al-Dhaifallah, H. Rezk, A low-grade heat Organic Rankine Cycle driven  
943 by hybrid solar collectors and a waste heat recovery system, *Energy Reports* 6 (2020) 3425–3445. doi:  
944 10.1016/j.egyr.2020.12.011.
- 945 [92] T. Li, Y. Zhang, H. Gao, X. Gao, F. Jin, Techno-economic-environmental performance of different system

- 946 configuration for combined heating and power based on organic rankine cycle and direct/indirect heating,  
947 *Renew. Energy* 219 (2023) 119553. doi:10.1016/j.renene.2023.119553.
- 948 [93] C. Mohd Noor, M. Noor, R. Mamat, Biodiesel as alternative fuel for marine diesel engine applications: A  
949 review, *Renew. Sust. Energ. Rev.* 94 (2018) 127–142. doi:10.1016/j.rser.2018.05.031.
- 950 [94] ANAVE (Asociación de navieros españoles), Precio de los combustibles marinos 2020-2024 (\$/t), Available  
951 online: <https://anave.es/precio-de-los-combustibles-marinos/>, (accessed on 21 Jul. 2024).
- 952 [95] E. Baldasso, J. G. Andreasen, M. E. Mondejar, U. Larsen, F. Haglind, Technical and economic feasibility of  
953 organic Rankine cycle-based waste heat recovery systems on feeder ships: Impact of nitrogen oxides emission  
954 abatement technologies, *Energy Convers. Manag.* 183 (2019) 577–589. doi:10.1016/j.enconman.2018.  
955 12.114.
- 956 [96] O. Konur, O. Yuksel, S. A. Korkmaz, C. O. Colpan, O. Y. Saatcioglu, I. Muslu, Thermal design and analysis  
957 of an organic rankine cycle system utilizing the main engine and cargo oil pump turbine based waste heats in a  
958 large tanker ship, *J. Clean. Prod.* 368 (2022) 133230. doi:10.1016/j.jclepro.2022.133230.
- 959 [97] H. Habibi, M. Zoghi, A. Chitsaz, K. Javaherdeh, M. Ayazpour, Thermo-economic analysis and optimization of  
960 combined PERC - ORC - LNG power system for diesel engine waste heat recovery, *Energy Convers. Manag.*  
961 173 (2018) 613–625. doi:10.1016/j.enconman.2018.08.005.
- 962 [98] G. Shu, P. Liu, H. Tian, X. Wang, D. Jing, Operational profile based thermal-economic analysis on an Organic  
963 Rankine cycle using for harvesting marine engine's exhaust waste heat, *Energy Convers. Manag.* 146 (2017)  
964 107–123. doi:10.1016/j.enconman.2017.04.099.
- 965 [99] Z. Wang, H. Chen, R. Xia, F. Han, Y. Ji, W. Cai, Energy, exergy and economy (3E) investigation of a SOFC-  
966 GT-ORC waste heat recovery system for green power ships, *Therm. Sci. Eng. Prog.* 32 (2022) 101342. doi:  
967 10.1016/j.tsep.2022.101342.
- 968 [100] A. G. Elkafas, Thermodynamic analysis and economic assessment of organic Rankine cycle integrated with  
969 thermoelectric generator onboard container ship, *Processes* 12 (2) (2024). doi:10.3390/pr12020355.